J|A|C|S
ARTICLES
Published on Web 03/22/2006

Direct Hydrogen-Atom Abstraction by Activated Bleomycin: An Experimental and Computational Study

Andrea Decker, Marina S. Chow, Jyllian N. Kemsley, Nicolai Lehnert, and Edward I. Solomon*

Contribution from the Department of Chemistry, Stanford University, Stanford, California 94305

Received October 28, 2005; E-mail: edward.solomon@stanford.edu

Abstract: Bleomycin (BLM), a glycopeptide antibiotic chemotherapy agent, is capable of single- and double-strand DNA damage. Activated bleomycin (ABLM), a low-spin $Fe^{III}-OOH$ complex, is the last intermediate detected prior to DNA cleavage following hydrogen-atom abstraction from the C-4′ of a deoxyribose sugar moiety. The mechanism of this C−H bond cleavage reaction and the nature of the active oxidizing species are still open issues. We have used kinetic measurements in combination with density functional calculations to study the reactivity of ABLM and the mechanism of the initial attack on DNA. Circular dichroism spectroscopy was used to directly monitor the kinetics of the ABLM reaction. These experiments yield a deuterium isotope effect, $k_H/k_D \approx 3$ for ABLM decay, indicating the involvement of a hydrogen atom in the rate-determining step. H-atom donors with relatively weak X−H bonds accelerate the reaction rate, establishing that ABLM is capable of hydrogen-atom abstraction. Density functional calculations were used to evaluate the two-dimensional potential energy surface for the direct hydrogen-atom abstraction reaction of the deoxyribose 4′-H by ABLM. The calculations confirm that ABLM is thermodynamically and kinetically competent for H-atom abstraction. The activation and reaction energies for this pathway are favored over both homolytic and heterolytic O−O bond cleavage. Direct H-atom abstraction by ABLM would generate a reactive $Fe^{IV}=O$ species, which would be capable of a second DNA strand cleavage, as observed *in vivo*. This study provides experimental and theoretical evidence for direct H-atom abstraction by ABLM and proposes an attractive mechanism for the role of ABLM in double-strand cleavage.

1. Introduction

Bleomycin (BLM, Figure 1), a glycopeptide antibiotic, is clinically used in cancer chemotherapy, especially against head, neck, and testicular cancers and Hodgkin's disease.[1−3] Its cytotoxic activity is believed to be due to its ability to carry out single- and especially double-strand cleavage of DNA in the presence of a reduced metal ion and dioxygen.[4−8] The highest activity *in vivo* is found for Fe^{II}BLM.[9]

BLM provides five or six ligands for binding to the iron. Because no crystal structure exists, current knowledge of the Fe−BLM structure is based on spectroscopy,[10−14] molecular dynamics modeling,[15] density functional calculations,[16,17] and studies on BLM complexes with Co,[18−21] Cu,[22,23] and other metals.[24−27] All studies agree on five nitrogen-based ligands (indicated in bold in Figure 1). The four equatorial ligands are generally accepted to be an imidazole nitrogen, a deprotonated amide, a pyrimidine nitrogen, and the secondary amine functionality of the β-aminoalanine. The primary amine of the β-aminoalanine has been proposed as an axial ligand.

Fe^{II}BLM reacts with dioxygen in the presence of reducing equivalents to form activated bleomycin (ABLM), the last intermediate detected prior to DNA strand scission.[4,28] It is well

(1) Umezawa, H. *Anticancer Agents based on Natural Products*;; Academic Press: New York, 1980.
(2) Carter, S. K. *Bleomycin Chemotherapy*; Academic Press: New York, 1985.
(3) Lazo, J. S.; Chabner, B. A. *Cancer Chemotherapy and Biotherapy: Principles and Practice*; Lippinkott-Raven: Philadelphia, PA, 1996.
(4) Hecht, S. M. *Acc. Chem. Res.* **1986**, *19*, 383−391.
(5) Stubbe, J.; Kozarich, J. W. *Chem. Rev.* **1987**, *87*, 1107−1136.
(6) Stubbe, J.; Kozarich, J. W.; Wu, W.; Vanderwall, D. E. *Acc. Chem. Res.* **1996**, *29*, 322−330.
(7) Burger, R. M. *Chem. Rev.* **1998**, *98*, 1153−1169.
(8) Hecht, S. M. *J. Nat. Prod.* **2000**, *63*, 158−168.
(9) Radtke, K.; Lornito, F. A.; Byrnes, R. W.; Antholine, W. E.; Petering, D. H. *Biochem. J.* **1994**, *302*, 655−664.
(10) Loeb, K. E.; Zaleski, J. M.; Westre, T. E.; Guajardo, R. J.; Mascharak, P. K.; Hedman, B.; Hodgson, K. O.; Solomon, E. I. *J. Am. Chem. Soc.* **1995**, *117*, 4545−4561.
(11) Lehmann, T. E.; Ming, L. J.; Rosen, M. E.; Que, L. *Biochemistry* **1997**, *36*, 2807−2816.
(12) Fulmer, P.; Zhao, C.; Li, W.; Derose, E.; Antholine, W. E.; Petering, D. H. *Biochemistry* **1997**, *36*, 4367−4374.
(13) Loeb, K. E.; Zaleski, J. M.; Hess, C. D.; Hecht, S. M.; Solomon, E. I. *J. Am. Chem. Soc.* **1998**, *120*, 1249−1259.
(14) Smolentsev, G.; Soldatov, A. V.; Wasinger, E. C.; Solomon, E. I. *Inorg. Chem.* **2004**, *43*, 1825−1827.
(15) Lehmann, T. E. *J. Biol. Inorg. Chem.* **2002**, *7*, 305−312.
(16) Freindorf, M.; Kozlowski, P. M. *J. Phys. Chem. A* **2001**, *105*, 7267−7272.
(17) Karawajczyk, A.; Buda, F. *J. Biol. Inorg. Chem.* **2005**, *10*, 33−40.
(18) Xu, R. X.; Nettesheim, D.; Otvos, J. D.; Petering, D. H. *Biochemistry* **1994**, *33*, 907−916.
(19) Lui, S. M.; Vanderwall, D. E.; Wu, W.; Tang, X. J.; Turner, C. J.; Kozarich, J. W.; Stubbe, J. *J. Am. Chem. Soc.* **1997**, *119*, 9603−9613.
(20) Lehmann, T. E.; Serrano, M. L.; Que, L. *Biochemistry* **2000**, *39*, 3886−3898.
(21) Fedeles, F.; Zimmer, M. *Inorg. Chem.* **2001**, *40*, 1557−1561.
(22) Sugiyama, M.; Kumagai, T.; Hayashida, M.; Maruyama, M.; Matoba, Y. *J. Biol. Chem.* **2002**, *277*, 2311−2320.
(23) Lehmann, T. E. *J. Biol. Inorg. Chem.* **2004**, *9*, 323−334.
(24) Mouzopoulou, B.; Kozlowski, H.; Katsaros, N.; Garnier-Suillerot, A. *Inorg. Chem.* **2001**, *40*, 6923−6929.
(25) Papakyriakou, A.; Katsaros, N. *Eur. J. Inorg. Chem.* **2003**, 3001−3006.
(26) Papakyriakou, A.; Mouzopoulou, B.; Katsaros, N. *J. Biol. Inorg. Chem.* **2003**, *8*, 549−559.
(27) Papakyriakou, A.; Bratsos, I.; Katsarou, M.; Katsaros, N. *Eur. J. Inorg. Chem.* **2004**, 3118−3126.

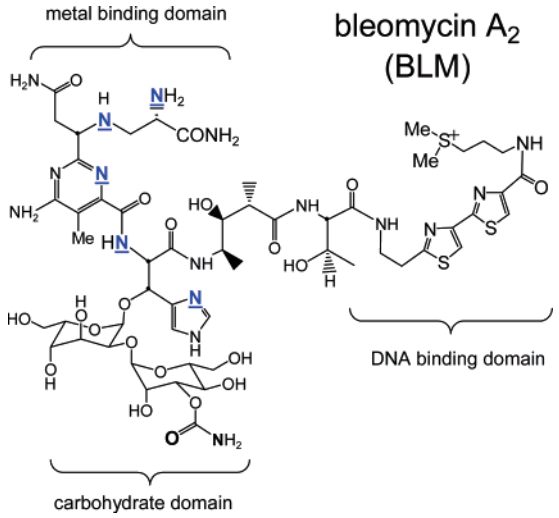

Figure 1. Structure of bleomycin (likely metal ligating atoms indicated in bold blue).

established by electron paramagnetic resonance (EPR) spectroscopy,[28−30] Mössbauer spectroscopy,[31] electron nuclear double-resonance (ENDOR) spectroscopy,[30,32] mass spectrometry,[33] X-ray absorption spectroscopy (XAS),[34] and magnetic circular dichroism (MCD) spectroscopy[35] that ABLM is a low-spin (ls) ferric-hydroperoxo complex, BLM−Fe^{III}−OOH.

ABLM can be formed when ferrous BLM, (BLM)Fe^{II}−OH_2, reacts with O_2 or when ferric BLM, (BLM)Fe^{III}−OH, reacts with excess H_2O_2.[28,36] Both pathways result in the same ABLM species,[28] and both generate the same DNA cleavage products.[36,37] In the absence of DNA, the decay of ABLM yields Fe^{III}BLM and water as final products.[28] The rate of ABLM decay is known to be first order in the concentration of ABLM. The half-life for the decay of ABLM has been measured to be ∼1.5 min at 0 °C in buffer (50 mM sodium cacodylate, pH 7.2)[37] and ∼2 min at 4−6 °C in unbuffered solution.[28] To understand the mechanism of ABLM decay, several studies have analyzed the decay products for reactive oxygen species, however with different results: one study did not detect peroxides (H_2O_2) or superoxides ($O_2^{\bullet-}$),[38] another identified small amounts of peroxides,[39] and a third observed only small amounts of hydroxy radicals ($^{\bullet}$OH) and superoxides.[40] The fluorescence of the BLM bithiazole tail was observed to be altered upon ABLM decay.[41] Kinetic studies of the formation and decay of ABLM have been challenging, since ABLM does not have a distinguishable spectroscopic absorption feature that can be easily monitored. Past studies involved freeze−quench methods to monitor changes to the EPR spectrum of ABLM, or the measurement of DNA cleavage ability of ABLM at set time points.[28,42]

There are two major DNA binding interactions for BLM. The bithiazole tail binds nonspecifically via partial intercalation[43,44] or through interactions with the minor grove.[45] Hydrogen-bonding interactions between the pyrimidine in the metal binding domain and the DNA guanine are thought to be responsible for the sequence specificity of DNA cleavage.[46−49] DNA strand scission is initiated through the abstraction of the C-4′ hydrogen atom of the backbone deoxyribose sugar[50,51] mainly at pyrimidine nucleotides of preferred sites containing 5′-GC and 5′-GT sequences.[52,53] After this initial attack, which generates a radical centered on the sugar C-4′, DNA cleavage can proceed via two pathways,[54−59] producing free bases independent of O_2 and base propenals when additional O_2 is available.

Although considerable research has been devoted to the reactivity of bleomycin, the nature of the active oxidizing species attacking the sugar C-4′ and the mechanism of this C−H bond cleavage reaction are still open issues. Three possible reaction pathways for the reactivity of ABLM in hydrogen-atom abstraction from DNA (Scheme 1) have been invoked: (1) Heterolytic cleavage of the O−O bond, generating a catalytically active "Fe^{V}═O" species, as has been observed in heme systems, where the formally "Fe^{V}═O" is stabilized by oxidation of the porphyrin ligand (Por), leading to a (Por$^{+\bullet}$)Fe^{IV}═O species ("compound I"). (2) Homolytic O−O bond cleavage, leading to a reactive Fe^{IV}═O intermediate and OH radical, as has been shown to occur for low-spin Fe^{III}OOH/R model systems and has been suggested to occur in mechanistic cycles of models of non-heme iron enzymes. (3) H-atom abstraction from the C-4′ of the DNA deoxyribose sugar directly by the hydroperoxo complex, ABLM.

(28) Burger, R. M.; Peisach, J.; Horwitz, S. B. *J. Biol. Chem.* **1981**, *256*, 11636−11644.
(29) Sugiura, Y. *J. Am. Chem. Soc.* **1980**, *102*, 5208−5215.
(30) Veselov, A.; Sun, H.; Sienkiewicz, A.; Taylor, H.; Burger, R. M.; Scholes, C. P. *J. Am. Chem. Soc.* **1995**, *117*, 7508−7512.
(31) Burger, R. M.; Kent, T. A.; Horwitz, S. B.; Münck, E.; Peisach, J. *J. Biol. Chem.* **1983**, *258*, 1559−1564.
(32) Veselov, A.; Burger, R. M.; Scholes, C. P. *J. Am. Chem. Soc.* **1998**, *120*, 1030−1033.
(33) Sam, J. W.; Tang, X.-J.; Peisach, J. *J. Am. Chem. Soc.* **1994**, *116*, 3250−5256.
(34) Westre, T. E.; Loeb, K. E.; Zaleski, J. M.; Hedman, B.; Hodgson, K. O.; Solomon, E. I. *J. Am. Chem. Soc.* **1995**, *117*, 1309−1313.
(35) Neese, F.; Zaleski, J. M.; Loeb Zaleski, K.; Solomon, E. I. *J. Am. Chem. Soc.* **2000**, *122*, 11703−11724.
(36) Kuramochi, H.; Takahashi, K.; Takita, T.; Umezawa, H. *J. Antibiot.* **1981**, *34*, 576−582.
(37) Natrajan, A.; Hecht, S. M.; van der marel, G. A.; van Boom, J. H. *J. Am. Chem. Soc.* **1990**, *112*, 3997−4002.
(38) Burger, R. M.; Horwitz, S. B.; Peisach, J.; Wittenberg, J. B. *J. Biol. Chem.* **1979**, *254*, 12299−12302.
(39) Oberley, L. W.; Buettner, G. R. *FEBS Lett.* **1979**, *97*, 47−49.
(40) Sugiura, Y.; Kikuchi, T. *J. Antibiot.* **1978**, *31*, 1310−1312.
(41) Nakamura, M.; Peisach, J. *J. Antibiot.* **1988**, *41*, 638−647.
(42) Burger, R. M.; Tian, G.; Drlica, K. *J. Am. Chem. Soc.* **1995**, *117*, 1167−1168.
(43) Povirk, L. F.; Hogan, M.; Dattagupta, N. *Biochemistry* **1979**, *18*, 96−101.
(44) Wu, W.; Vanderwall, D. E.; Stubbe, J.; Kozarich, J. W.; Turner, C. J. *J. Am. Chem. Soc.* **1994**, *116*, 10843−10844.
(45) Abraham, A. T.; Zhou, X.; Hecht, S. M. *J. Am. Chem. Soc.* **2001**, *123*, 5167−5175.
(46) Wu, W.; Vanderwall, D. E.; Turner, C. J.; Kozarich, J. W.; Stubbe, J. *J. Am. Chem. Soc.* **1996**, *118*, 1281−1294.
(47) Vanderwall, D. E.; Lui, S. M.; Wu, W.; Turner, C. J.; Kozarich, J. W.; Stubbe, J. *Chem. Biol.* **1997**, *4*, 373−387.
(48) Boger, D. L.; Ramsey, T. M.; Cai, H.; Hoehn, S. T.; Kozarich, J. W.; Stubbe, J. *J. Am. Chem. Soc.* **1998**, *120*, 53−65.
(49) Kemsley, J. N.; Zaleski, K. L.; Chow, M. S.; Decker, A.; Shishova, E. Y.; Wasinger, E. C.; Hedman, B.; Hodgson, K. O.; Solomon, E. I. *J. Am. Chem. Soc.* **2003**, *125*, 10810−10821.
(50) Wu, J. C.; Kozarich, J. W.; Stubbe, J. *Biochemistry* **1985**, *24*, 7562−7568.
(51) Worth, L.; Frank, B. L.; Christner, D. F.; Absalon, M. J.; Stubbe, J.; Kozarich, J. W. *Biochemistry* **1993**, *32*, 2601−2609.
(52) Takeshita, M.; Grollman, A. P.; Ohtsubo, E.; Ohtsubo, H. *Proc. Natl. Acad. Sci. U.S.A.* **1978**, *75*, 5983−5987.
(53) D'Andrea, A. D.; Haseltine, W. A. *Proc. Natl. Acad. Sci. U.S.A.* **1978**, *75*, 3608−3612.
(54) Haidle, C. W.; Weiss, K. K.; Kuo, M. T. *Mol. Pharmacol.* **1972**, *8*, 531−537.
(55) Povirk, L. F.; Wübker, W.; Köhnlein, W.; Hutchinson, F. *Nucleic Acids Res.* **1977**, *4*, 3573−3580.
(56) Povirk, L. F.; Köhnlein, W.; Hutchinson, F. *Biochim. Biophys. Acta* **1978**, *521*, 126−133.
(57) Burger, R. M.; Berkowitz, A. R.; Peisach, J.; Horwitz, S. B. *J. Biol. Chem.* **1980**, *255*, 11832−11838.
(58) Giloni, L.; Takeshita, M.; Johnson, F.; Iden, C.; Grollman, A. P. *J. Biol. Chem.* **1981**, *256*, 8608−8615.
(59) Breen, A. P.; Murphy, J. A. *Free Radical Biol. Bed.* **1995**, *18*, 1033−1077.

Scheme 1. Possible Reaction Pathways for ABLM

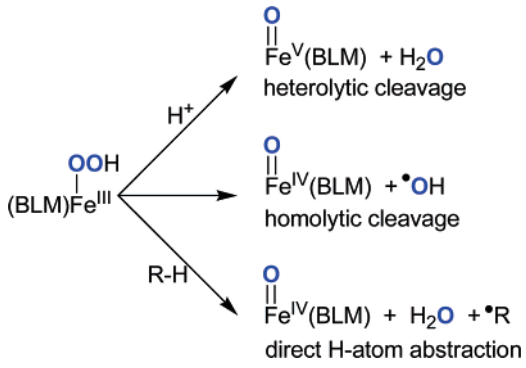

Pathway 1 is reminiscent of the activation and mechanism of the heme enzyme cytochrome P450 and has been proposed due to the strong similarity between the chemistry of ABLM and that of P450 (i.e., H-atom abstraction from unactivated C−H bonds, hydroxylation, and epoxidation).[60−63] However, a detailed quantum chemical study on the electronic structure of ABLM and its reactivity[35] suggested strongly that heterolytic O−O bond cleavage is energetically unfavorable, less favorable for BLM than for heme systems by at least 70 kcal/mol.[64] Heterolytic cleavage would lead to a product which is best described as a $(BLM^{\bullet+})Fe^{IV}{=}O$ with the hole localized on the deprotonated amide, in contrast to the heme compound I species, where the hole is delocalized over the porphyrin ring. Ligand-to-metal charge-transfer (LMCT) spectra show experimentally that it is energetically much harder to remove an electron from the bleomycin ligand than from the porphyrin ring,[35,65] making heterolytic O−O bond cleavage in BLM energetically much less favorable.

Pathway 2 was evaluated by studying the electronic structures and reactivities of ls ferric−alkylperoxo[66] and −hydroperoxo[67] model complexes. The bonding of ls Fe^{III}−OOH is characterized by strong Fe−O and weak O−O bonds. This species is thermodynamically and kinetically competent to undergo homolytic cleavage of the O−O bond to yield $Fe^{IV}{=}O$ and •OH. DFT studies of the reaction mechanism show no additional activation barrier along the reaction coordinate.[68] A parallel study on the homolytic cleavage of ABLM gave similar results: Theoretically, ABLM is thermodynamically and kinetically competent to homolytically cleave the O−O bond with a calculated reaction free energy of $\Delta G = 13$ kcal/mol and no additional kinetic activation barrier.[67]

However, the fact that initial attack occurs through specific hydrogen-atom abstraction only from the C-4′ on the deoxyribose sugar,[69,70] with an isotope selection effect $k_H/k_D = 2-7$,[51] argues against an involvement of the very reactive and unselective hydroxyl radical (produced in homolytic O−O bond cleavage). A large tritium selection effect observed for the reaction of ABLM with a DNA model poly(dA-dU) provides evidence for the involvement of C−H bond cleavage in the rate-determining step.[50] On the other hand, ^{18}O isotope studies[42] demonstrate that the O−O bond cleavage is also involved in the rate-determining step.

The proposed third pathway suggests that ABLM itself is the active oxidizing species which directly abstracts the hydrogen atom. A comparison of the reaction energies of the three proposed pathways for ABLM shows that the reaction energies for homolytic and heterolytic cleavage are comparable and endergonic ($\Delta G \approx 13$ kcal/mol). The direct H-atom abstraction is exergonic ($\Delta G = -7$ kcal/mol) and thus thermodynamically favored.[64]

The present investigation extends these studies on the reactivity of ABLM and evaluates with experimental and computational methods the kinetics of a direct H-atom abstraction reaction by ABLM. Since ABLM does not have a characteristic absorption feature that can be easily monitored, kinetic studies of ABLM decay have been challenging. However, using circular dichroism (CD) spectroscopy, we have identified such a feature and have measured the kinetics of ABLM decay and its reaction with hydrogen-atom donor substrates through deuterium isotope studies. Furthermore, density functional calculations were used to map the two-dimensional potential energy surface (PES) for the direct hydrogen-atom abstraction reaction by ABLM (one dimension being the cleavage of the O−O bond, the second dimension the transfer of the hydrogen atom). In addition, we propose a mechanism for initiating the second strand cleavage event and contrast the direct H-atom abstraction pathway to the heterolytic O−O bond cleavage pathway.

This study provides new insight into the reaction mechanism of ABLM on a molecular level and the effectiveness of this anti-cancer drug in DNA cleavage.

2. Methods

2.1. Experimental Procedures. 2.1.1. Fe^{II}BLM. Solutions of ferrous bleomycin were prepared under strict anaerobic conditions. Bleomycin sulfate (Calbiochem) was evacuated and back-filled with argon 20 times in a Teflon-capped conical vial. $Fe^{II}(NH_4)_2(SO_4)_2{\cdot}6H_2O$ (Fe^{II}AS, J.T. Baker) was purged with argon for 2 h. HEPES buffer (100 mM, Sigma) was prepared in deionized water and adjusted to pH 7.8 with NaOH. Deionized water and HEPES buffer were degassed by 5−10 freeze−pump−thaw cycles at 10^{-3} Torr in Teflon- and ground-glass-stoppered flasks. All degassed materials were immediately placed into a Vacuum Atmospheres Nexus-1 anaerobic glovebox (<5 ppm oxygen). Approximately 0.9 equiv of aqueous Fe^{II}AS was added anaerobically to a solution of bleomycin in HEPES buffer. The salmon-pink-colored Fe^{II}-BLM solutions were either kept on a cold plate during use or frozen and stored in liquid nitrogen. Stock solutions typically contained 5 mM Fe^{II} and 5.6 mM BLM.

2.1.2. ABLM. Activated bleomycin (ABLM) was generated by addition of oxygenated HEPES buffer to anaerobic Fe^{II}BLM according to the equation

(60) Padbury, G.; Sligar, S. G. *J. Biol. Chem.* **1985**, *260*, 7820−7823.
(61) Murugesan, N.; Hecht, S. M. *J. Am. Chem. Soc.* **1985**, *107*, 493−500.
(62) Heimbrook, D. C.; Carr, S. A.; Mentzer, M. A.; Long, E. C.; Hecht, S. M. *Inorg. Chem.* **1987**, *26*, 3835−3836.
(63) Ehrenfeld, G. M.; Murugesan, M.; Hecht, S. M. *Inorg. Chem.* **1984**, *23*, 1496−1498.
(64) Solomon, E. I.; Decker, A.; Lehnert, N. *Proc. Natl. Acad. Sci. U.S.A.* **2003**, *100*, 3589−3594.
(65) Cheesman, M. R.; Greenwood, C.; Thomson, A. J. *Adv. Inorg. Chem.* **1991**, *36*, 201−255.
(66) Lehnert, N.; Ho, R. Y. N.; Que, L., Jr.; Solomon, E. I. *J. Am. Chem. Soc.* **2001**, *123*, 8271−8290.
(67) Lehnert, N.; Ho, R. Y. N.; Neese, F.; Que, L., Jr.; Solomon, E. I. *J. Am. Chem. Soc.* **2002**, *124*, 10810−10822.
(68) Lehnert, N.; Ho, R. Y. N.; Que, L., Jr.; Solomon, E. I. *J. Am. Chem. Soc.* **2001**, *123*, 12802−12816.
(69) Wu, J. C.; Kozarich, J. W.; Stubbe, J. *J. Biol. Chem.* **1983**, *258*, 4694−4697.
(70) Kozarich, J. W.; Worth, L., Jr.; Frank, B. L.; Christner, D. F.; Vanderwall, D. E.; Stubbe, J. *Science* **1989**, *245*, 1396−1399.

$$2Fe^{II}BLM + O_2 \rightarrow Fe^{III}BLM + ABLM$$

In the glovebox, aliquots of $Fe^{II}BLM$ were transferred into gastight Teflon-capped quartz cuvettes. Just before use, a cuvette was taken out of the glovebox and inserted into a temperature-controlled cuvette holder in the CD instrument. Oxygenated HEPES buffer and/or substrate was injected into the cuvette as data collection was started. CD spectra were collected on a Jasco J810 spectrophotometer using an S1 photomultiplier tube detector and the Jasco Spectra Manager program interface.

Scans from 11 100−33 300 cm^{-1} (900−300 nm) were collected at approximately 20 s intervals until no further change was observed (~15 min). From these spectra, it was determined that the greatest change in the CD spectrum occurred at 22 200 cm^{-1} (450 nm). The CD intensity at 22 200 cm^{-1} was then monitored over 20 min to yield ABLM decay kinetics.

2.1.3. Substrates. Ascorbic acid (Sigma) and 4-hydroxy-tetramethyl-piperidine-1-oxyl (4-hydroxy-TEMPO•, Sigma) were purged with argon. Ascorbic acid was dissolved in degassed water and used within 4 h. To prepare 4-hydroxy-TEMPO−H, between 0.25 and 1 equiv of ascorbic acid was anaerobically reacted with 4-hydroxy-TEMPO• according to the equation

$$\text{4-hydroxy-TEMPO}^{\bullet} + AscH^{-} \rightarrow \text{4-hydroxy-TEMPO−H} + Asc^{-\bullet}$$

$$2Asc^{-\bullet} \rightarrow AscH^{-} + DHA$$

(where DHA is dehydroascorbic acid). The orange 4-hydroxy-TEMPO• solution turned colorless when ascorbate acid was added. To quantify the conversion of 4-hydroxy-TEMPO• to 4-hydroxy-TEMPO−H, the disappearance of the 4-hydroxy-TEMPO• radical signal was monitored at room temperature by EPR spectroscopy (Bruker 220-D SRC). The percentage decrease in EPR signal intensity of the 4-hydroxy-TEMPO• species can be correlated to the percent conversion of 4-hydroxy-TEMPO• to 4-hydroxy-TEMPO−H in its reaction with ascorbate. When 4-hydroxy-TEMPO• was reacted with 0.5 molar equiv of ascorbate, the intensity of the radical EPR signal was observed to decrease by between 96 and 99%. Therefore, the addition of 0.5 molar equiv of ascorbic acid produced 96−99% 4-hydroxy-TEMPO−H while minimizing (by stoichiometry) ascorbate as a side product (Supporting Information, SI-1).

2.1.4. ABLM Reactions. Varying amounts (between 20 and 100 equiv) of 4-hydroxy-TEMPO−H and ascorbate were loaded into gastight Hamilton syringes, taken out of the glovebox, and transported to the CD spectrophotometer. Repetitive spectral scans and single-wavelength kinetics data were collected as described above. A known amount of substrate was injected into the airtight CD cuvette within 1−2 s after the injection of oxygen-saturated buffer. The concentration of $Fe^{II}BLM$ was typically 0.3 mM, with substrate concentrations between 6 and 30 mM. Kinetic measurements were repeated at least three times for each concentration of substrate used. Control experiments were performed where ABLM was reacted with 100 equiv each of dehydroascorbic acid (DHA) and 4-hydroxy-TEMPO•. These decay products did not affect the rate of ABLM decay.

The rate of ABLM decay as a function of temperature was measured between 5 and 30 °C. Between kinetic measurements, the oxygenated HEPES buffer (90−96% volume of reaction mixture) was submerged in the recirculating water bath that was also attached to the CD cell holder to ensure an accurate and constant reaction temperature.

For deuterium isotope studies, all solutions were prepared in D_2O (99.9 atom % D, Cambridge Isotope Labs). When anaerobicity was required, D_2O was degassed by 5−10 freeze−pump−thaw cycles. For deuterated HEPES buffer, the pD was taken as the pH meter reading + 0.4.[71] Stock solutions of $Fe^{II}BLM$ (5.0 mM Fe^{II}) prepared in degassed D_2O were allowed to equilibrate anaerobically for 1−2 h before use.

(71) Schowen, K. B. In *Solvent Hydrogen Isotope Effects*; Schowen, K. B., Ed.; Plenum Press: New York, 1978; pp 225−283.

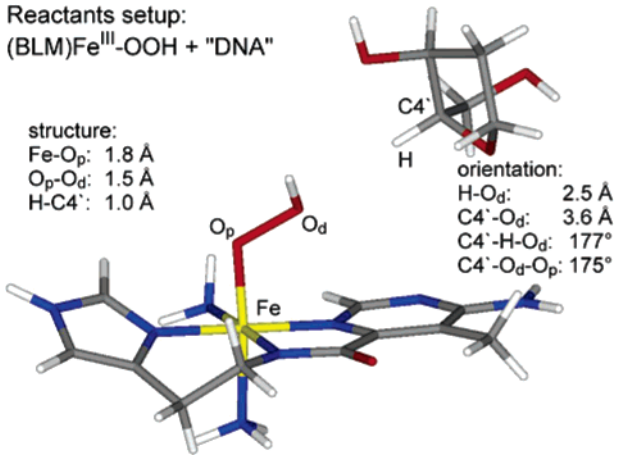

Figure 2. Setup and orientation of reactants ABLM and deoxyribose sugar (for a stereopair of this figure, see Supporting Information).

2.2. Computational Methods. Spin-unrestricted density functional theory (DFT) calculations were performed with the Gaussian 03 program package.[72] Becke's three-parameter hybrid functional with the correlation functional of Lee, Yang, and Parr (B3LYP)[73,74] was used. The LanL2DZ basis set, which applies Dunning/Huzinaga full double-ζ (D95) basis functions[75] on first-row elements and Los Alamos effective core potentials plus DZ functions[76−78] on all other atoms, was used in all geometry optimizations. Orbitals were plotted using Molden.[79]

2.2.1. Reaction Energies. To determine the thermodynamic parameters, the geometries of all reactant and product species have been fully optimized without constraints, and the frequencies were found to be real in all cases. All energies were obtained from single-point calculations on the LanL2DZ-optimized structures using the following larger basis set: The atoms directly involved in the reaction (Fe−O−O−H; H−C in all reactant and product species) were described by a large triple-ζ basis set including polarization and diffuse functions on heavy atoms and hydrogens, 6-311++G(3df,pd) in Gaussian. The nitrogens of the bleomycin ligand directly ligated to the iron were described by a triple-ζ basis set including a polarization function, 6-311G*. All other atoms were described by an all-electron double-ζ basis set, 6-31G*. The energies given include zero-point and thermal corrections. Solvation effects were considered using the polarized continuum model (PCM) as implemented in Gaussian 03 with a dielectric constant $\epsilon = 4.0$ to model the polypeptide and DNA environment of bleomycin. In all calculations, convergence was defined to occur when the relative change in the density matrix between subsequent iterations was $<1 \times 10^{-8}$.

2.2.2. The Models. The model for ABLM was taken from ref 35, which was constructed on the basis of spectroscopic data. The metal binding domain containing the pyrimidine, deprotonated amide, and imidazole moieties is completely retained; the primary and secondary amine ligands are modeled as NH_3's (Figure 2, left). The geometry was fully optimized, which has been shown to change the overall structure only slightly (model ABLM in ref 67) and not to significantly affect the reaction energies.[67] The low-spin $S = {}^1/_2$ ground state of this ferric−hydroperoxo species is reproduced in the calculations; the high-spin ($S = {}^5/_2$) state is 10 kcal/mol higher in energy. Similarly, the $(BLM)Fe^{IV}$=O, $(BLM)Fe^{V}$=O, and $(BLM)Fe^{III}$—OH species are low-

(72) Frisch, M. J.; et al. *Gaussian 03*, Revision C.02; Gaussian, Inc.: Wallingford, CT, 2004.
(73) Becke, A. D. *Phys. Rev. A* **1988**, *38*, 3098−3100.
(74) Becke, A. D. *J. Chem. Phys.* **1993**, *98*, 5648−5652.
(75) *Modern Theoretical Chemistry*, Dunning, T. H., Jr., Hay, P. J., Schaefer, H. F., III, Eds.; Plenum: New York, 1976.
(76) Hay, P. J.; Wadt, W. R. *J. Chem. Phys.* **1985**, *82*, 270−283.
(77) Hay, P. J.; Wadt, W. R. *J. Chem. Phys.* **1985**, *82*, 299−310.
(78) Wadt, W. R.; Hay, P. J. *J. Chem. Phys.* **1985**, *82*, 284−298.
(79) Schaftenaar, G.; Noordik, J. H. *J. Comput.-Aided Mol. Design* **2000**, *14*, 123−134 (http://www.cmbi.ru.nl/molden/molden.html).

spin, $S = 1$, $S = {}^1/_2$, and $S = {}^1/_2$, respectively, with the high-spin states ($S = 2$, $S = {}^3/_2$, and $S = {}^5/_2$) 13, 4, and 6 kcal/mol higher in energy.[80] Considering that the hybrid functional B3LYP in general favors high-spin over low-spin states, we are confident the calculations result in the correct ground state, and we have therefore focused on the low-spin reaction surface.

To model the natural substrate of ABLM, DNA, the deoxyribose sugar moiety was kept in its entirety, the 3′- and 5′-phosphates were substituted by hydroxy ligands, and the base was replaced by a hydrogen atom (Figure 2, right).

An extended model of the bleomycin ligand that includes the whole metal binding domain and part of the peptide linker region (see Supporting Information) was additionally used to ascertain the electronic structure of the putative "Fe^{V}═O" product and energetics of the heterolytic cleavage reaction. The optimized geometric structure is not significantly different compared to the smaller model.

2.2.3. H-Atom Abstraction (and Homolysis) by ABLM. The orientation of ABLM relative to the DNA deoxyribose sugar was adapted from solution NMR structures of (BLM)Co^{III}−OOH bound to oligonucleotides.[46,81] These structures show the hydroperoxo group pointing toward the hydrogen atom on the C-4′; molecular modeling revealed a distance of 2.5 Å between the distal oxygen of the hydroperoxide and the 4′-hydrogen.[46] Figure 2 shows the reactant orientation adopted here.

During the reaction scans, partial optimizations were carried out to allow for structural changes between reactants and products. At each step the following parameters of the BLM complex have been reoptimized: bond lengths and angles of the two NH_3's bound to the iron center, the Fe−O_p bond length, and all parameters of the hydroperoxo hydrogen atom. The structure of the sugar moiety was partially optimized to allow for structural changes associated with the transition from the sp^3 C-4′ to the radical product with an sp^2 C-4′. All lengths and angles of bonds connected to C-4′ and both C−OH bond lengths of the terminal hydroxy groups were allowed to adjust. The 4′-hydrogen parameters were optimized during the scans of the O_p−O_d distance. These partial optimizations result in product species, (BLM)Fe^{IV}═O, H_2O, and a C-4′ sugar radical, which are structurally and energetically very similar to the fully optimized structures (energetic error less than 2 kcal/mol).

To construct the two-dimensional potential energy surface, the following reaction coordinates were scanned.

scan r(O−O) − fix r(O_d−C-4′): Stepwise scan elongating the O_p−O_d distance from r(O−O) = 1.5 Å, which is the optimized bond length in ABLM, to r(O−O) = 4.5 Å. The distance between ABLM and the substrate was held constant at r(O_d−C-4′) = 2.5 Å, the distance taken from the solution NMR structure. The position of the 4′-hydrogen atom was reoptimized at each step (purple line in 2D-PES, Figure 9).

scan r(O−O) − opt r(O_d−C-4′): To take into account the flexibility of the ABLM-DNA binding, the distance to the substrate, r(O_d−C-4′), was reoptimized while the O−O bond length was increased stepwise from r(O−O) = 1.5 Å to r(O−O) = 2.7 Å. The distance between the peroxo ligand and the sugar, including the hydrogen atom, decreases gradually, until at r(O−O) > 2.7 Å the 4′-hydrogen moves spontaneously to the distal oxygen, forming the products H_2O and sugar radical (red curve in 2D-PES, Figure 9).

scan r(O−H) − opt r(O_d−C-4′): At selected, fixed O_p−O_d distances (1.8, 2.0, 2.2, 2.4, 2.5, 2.6, 2.7, 2.9, and 3.1 Å), the 4′-hydrogen atom was not optimized but transferred stepwise from the C-4′ to the distal oxygen of the hydroperoxo, until the optimized bond length of r(O−H) = 1.1 Å was reached. The distance between the peroxo unit and the substrate, r(O_d−C-4′), was reoptimized at each step, analogous to the *r(O−O) − opt r(O_d−C-4′)* scan. On the potential energy surface, these scans run perpendicular to the scan elongating the O−O bond length.

A saddle point search without any constraints yielded the transition state for this reaction. It has only one imaginary frequency of −195 cm^{-1}. The vibrational mode of this frequency includes the distal oxygen as well as the 4′-hydrogen moving along the common reaction pathway. The energy of the transition state was calculated using the large triple-ζ basis set described above and included solvent effects and zero-point energy and thermal corrections.

2.2.4. H-Atom Abstraction by (BLM)Fe^{IV}═O: Proposed Second Strand Cleavage Attack. For the reaction coordinate of the 4′-hydrogen-atom abstraction by (BLM)Fe^{IV}═O, a bleomycin−substrate starting orientation comparable to that of the first H-atom abstraction reaction described above was chosen. A similar orientation was found in an NMR structure of (BLM)Co^{III}−OOH bound to oligonucleotides with a mature strand lesion.[82] The same parameters as described above have been reoptimized at each step along the reaction scan to allow for structural changes between reactants and products, and the geometry of the transition state (*vide infra*) was determined without any structural constraints.

scan r(O−H) − opt r(O−C-4′): Along the reaction coordinate, the 4′-hydrogen has been transferred stepwise from the C-4′ of the sugar to the oxygen atom of the (BLM)Fe^{IV}═O reactant, forming the sugar radical and low-spin (BLM)Fe^{III}−OH. The distance between the C-4′ and the oxygen was optimized at each step.

A saddle point search without any constraints yielded the transition state, which has only one imaginary frequency of −1552 cm^{-1}. The vibrational motion corresponds to the hydrogen atom moving between the C-4′ of the sugar and the oxygen atom on the (BLM)Fe^{IV}═O.

2.2.5. Heterolytic O−O Bond Cleavage. The possibility of a heterolytic cleavage of the O−O bond coupled to a protonation of the leaving OH^- to produce a formally (BLM)Fe^{V}═O species and H_2O was evaluated.

Two proton sources were considered: (1) A solvated proton, H^+(solv), whose energy, $\Delta G_{solv}(H^+) = -262.23$ kcal/mol, has been determined by large-scale ab initio calculations on small water clusters $(H_2O)_n$.[83] (2) NH_4^+, a weak acid with pK_a = 9.25, has been used as an alternative proton source in order to be able to include the protonation step in the reaction. Both proton sources yield very similar reaction energies in a solvent environment and thus can be considered equivalent.

Using NH_4^+ as the proton source and starting from the fully optimized ABLM + NH_4^+ reactants, one possible reaction pathway for protonation and heterolytic O−O bond cleavage was followed.

scan r(O−H) − opt r(O−O) − opt r(O−N): Stepwise scan reducing the distance between one of the hydrogens on the NH_4^+, H_p, and the distal oxygen, O_d, of the hydroperoxide ABLM from the optimized distance r(O_d−H_p) = 1.5 Å to r(O_d−H_p) = 1.0 Å. Only five parameters have been fixed during this scan: the angle and dihedral angle of this hydrogen H_p, the angle and dihedral angle of the proximal oxygen, O_p, and the distance between the hydroperoxo hydrogen and the distal oxygen, O_d.[84] All of the bleomycin ligand and the O_p−O_d bond, angle, and dihedral angle were allowed to optimize at each step.

scan r(O−O): Subsequently, the O_p−O_d distance was elongated stepwise, starting with the optimized value at the end of the previous scan, r(O−O) = 1.5 Å, until the O−O distance reached r(O−O) = 4.5 Å. Now both hydrogens on the distal oxygen were fixed at r(O_d−H) = 1.02 Å. The distance to the NH_3 was optimized as well as all the other parameters from the previous scan.

(80) Neither the $S = 0$ spin state for the FeIV═O species, nor the intermediate spin $S = {}^3/_2$ for both of the ferric species, are considered, since these are energetically very unfavorable.

(81) Zhao, C.; Xia, C.; Mao, Q.; Forsterling, H.; DeRose, E.; Antholine, W. E.; Subczynski, W. K.; Petering, D. H. *J. Inorg. Biochem.* **2002**, *91*, 259−268.

(82) Hoehn, S. T.; Junker, H. D.; Bunt, R. C.; Turner, C. J.; Stubbe, J. *Biochemistry* **2001**, *40*, 5894−5905.

(83) Tawa, G. J.; Topol, I. A.; Burt, S. K.; Caldwell, R. A.; Rashin, A. A. *J. Chem. Phys.* **1998**, *109*, 4852−4863.

(84) When this parameter is allowed to optimize, the hydrogen moves from the distal oxygen of the peroxo, protonating the nitrogen of the deprotonated amide and resulting in a ferric−hydroperoxo species.

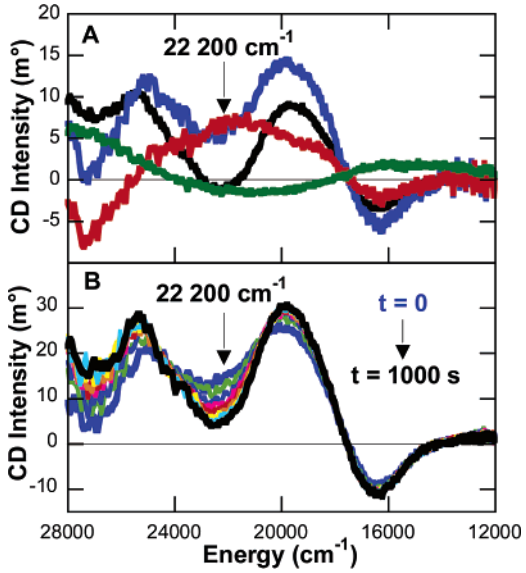

Figure 3. UV−vis CD spectra from 11 100 to 33 300 cm^{-1} (900−300 nm). (A) Spectra of Fe^{II}BLM (green), Fe^{III}BLM (black), and the initial reaction mixture containing 50% Fe^{III}BLM and 50% ABLM (blue). The ABLM spectrum (red) was obtained by subtracting the Fe^{III}BLM component from the spectrum of the reaction mixture. (B) Consecutive scans of the reaction mixture taken at 20 s intervals for 15 min. Spectra were collected at 5 °C.

3. Results and Analysis

3.1. ABLM Kinetics Studies. 3.1.1. Unimolecular Decay. When O_2 is added to anaerobic Fe^{II}BLM, oxy-BLM is formed, which disproportionates to give Fe^{III}BLM and (BLM)Fe^{III}−OOH (ABLM). Based on this reaction stoichiometry, it is possible to obtain the CD spectrum of ABLM (Figure 3A, red) by subtraction of the Fe^{III}BLM component from the spectrum of the reaction mixture and renormalization. The room-temperature CD spectrum of ABLM has a characteristic feature at ~22 200 cm^{-1} (~450 nm) that is absent in both Fe^{III}BLM[35] and Fe^{II}BLM[10] (black and green respectively in Figure 3A). At the concentrations used in these experiments, this band is too weak to be observed by absorption spectroscopy but is sufficiently intense in CD to allow direct monitoring of the ABLM reaction. The intensity of the ABLM band increases when oxygenated buffer is added to anaerobic Fe^{II}BLM, and at 20 °C it reaches a maximum approximately 10 s after the addition of oxygenated buffer. The band then decreased in intensity over time; no further change was observed after a period of 20 min. Figure 3B shows scans of the ABLM reaction mixture taken at 20 s intervals.

The rate of decay of ABLM was obtained by monitoring the decrease in intensity of the 22 200 cm^{-1} (450 nm) band as a function of time. An example of the ABLM decay curves obtained is shown in Figure 4 (solid lines). The data were fit to a single-exponential decay, $y = A_{initial} - \Delta A(1 - e^{-kt})$, where k is the observed rate constant. A fixed concentration of 0.3 mM Fe^{II}BLM was used throughout this study. At 5 °C, the observed rate constant of ABLM decay, $k_{ABLM(obs)}$, was determined to be 0.006 s^{-1}. This translates into an ABLM decay half-life ($t_{1/2}$) of ~1.9 min, which is in good agreement with reported $t_{1/2}$ values of ~2 min at 6 °C and ~1.5 min at 0 °C previously determined by EPR spectroscopy[28] and activity changes,[37] respectively.

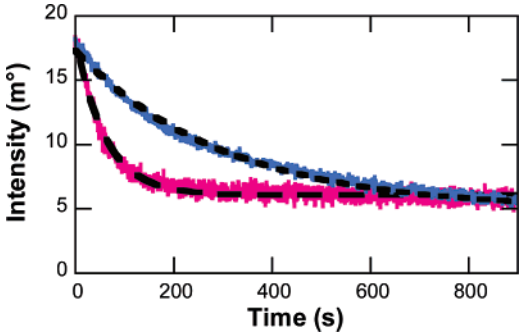

Figure 4. Representative CD traces at 22 200 cm^{-1} (450 nm) for the decay of ABLM at 5 °C. The red line represents decay of ABLM in H_2O, and the blue line represents decay of ABLM in D_2O. Dashed lines show the $y = A_{initial} - \Delta A(1 - e^{-kt})$ fits to the data.

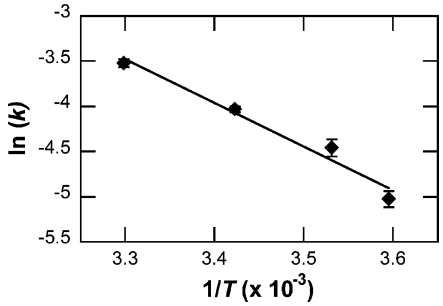

Figure 5. Temperature dependence of ABLM decay at 5, 10, 20, and 30 °C. The experimentally derived activation energy is 9.3 ± 0.9 kcal/mol.

Temperature Dependence. The temperature (T) dependence of the rate of ABLM decay is shown in Figure 5. The rate of ABLM decay was measured at least three times at each temperature. The data were fit to the Arrhenius equation, $k = A\ e^{-E_a/RT}$, where a plot of ln(k) against $1/T$ yields a slope $-E_a/R$. The experimentally derived activation energy for ABLM decay was 9.3 ± 0.9 kcal/mol, and the pre-exponential factor A was found to be on the order of 10^5. The standard deviation for E_a was obtained by varying the linear fit to the data.

Deuterium Isotope Effects. Deuterated Fe^{II}BLM was prepared and incubated for 1−2 h before use to ensure that all exchangeable hydrogens on the BLM molecule were replaced by deuterium atoms. These hydrogens are likely to be in O−H and N−H positions, which have been shown to have H/D exchange half-lives on the order of minutes in small molecules.[85,86] A representative trace of the ABLM decay in D_2O is shown in blue in Figure 4. At 20 °C, the rate constant of ABLM decay, $k_{ABLM(obs)}$, was 0.018 ± 0.003 s^{-1} when ABLM was prepared in H_2O and 0.005 ± 0.001 s^{-1} when ABLM was prepared in D_2O. This yields a kinetic isotope effect ($k_{ABLM(obs,H)}/k_{ABLM(obs,D)}$) of 3.6 ± 0.9, which is consistent with exchangeable H-atom involvement in the rate-determining step of ABLM decay.

The CD spectrum of the ABLM decay product is identical to that of Fe^{III}BLM. This is consistent with previous studies, showing that the product of ABLM decay is indistinguishable from Fe^{III}BLM by EPR and optical spectroscopy.[28] These results indicate that the ligand fields are the same in the Fe^{III}BLM species and the ABLM decay product. Hence, the H-atom abstracted during ABLM decay must be an exchangeable N−H

(85) Fersht, A. *Structure and Mechanism in Protein Science*; W. H. Freeman: New York, 1999; p 563.
(86) Arrington, C. B.; Robertson, A. D. *J. Mol. Biol.* **2000**, *296*, 1307−1317.

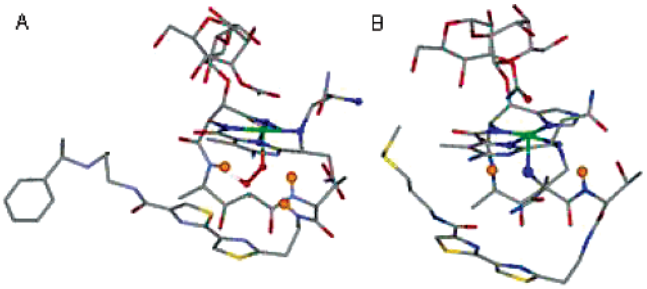

Figure 6. 3D NMR structures of (A) (Peplomycin)Co^{III}−OOH. Hydrogen atoms within 3 Å of the OOH moiety are highlighted as orange balls. Reproduced from PDB 1AO4.[87] (B) Co^{II}BLM (PDB 1DEY),[20] where highlighted H-atoms (orange balls) are ∼4 Å from the metal center. (Stereopairs of these structures can be found in the Supporting Information.)

or O−H atom from a non-ligand moiety on the BLM molecule. While no NMR solution structures of (BLM)Fe^{III}−OOH and (BLM)Co^{III}−OOH are available, they are known for two related species: Co^{III}−OOH bound to Peplomycin, a bleomycin analogue, and Co^{II}BLM. The (Peplomycin)Co^{III}−OOH NMR structure (Figure 6A) shows three amide N−H bonds that are within 3 Å of the −OOH moiety. In the closely related Co^{II}BLM structure (Figure 6B), two of these amide N−H bonds are within 4 Å of the metal center. These N−H bonds are highlighted in orange.

3.1.2. H-Atom Donor: 4-Hydroxy-TEMPO−H. To further test the hypothesis that ABLM is capable of reaction via an H-atom abstraction mechanism, we reacted ABLM with 4-hydroxy-TEMPO−H, which has one weak O−H bond of approximately 72 kcal/mol and is known to be a good H-atom donor. Control experiments showed no effect of dehydroascorbic acid, DHA (present in the reaction mixture from ascorbate reduction of 4-hydroxy-TEMPO•), on the rate of ABLM decay. 4-Hydroxy-TEMPO−H is found to be stable in the presence of oxygen and does not have a CD signal in the region of interest.

ABLM was reacted with 20−100 equiv of 4-hydroxy-TEMPO−H. The rate of reaction was found to be accelerated by increasing the concentration of substrate. A plot of the observed rate constants k_{obs} against concentration of 4-hydroxy-TEMPO−H is shown in Figure 7A (circles). The kinetic data were best fit by a straight line with vertical intercept at $k_{ABLM(obs,H)}$ of 0.018 s^{-1}, which corresponds to the observed rate constant of decay of ABLM in the absence of substrate (vide supra). The slope of the best-fit line yields the rate constant k_{2H} = 1.19 ± 0.09 M^{-1} s^{-1} for the ABLM decay pathway involving substrate. The rate expression for the rate-limiting reaction of ABLM with 4-hydroxy-TEMPO−H can be written as

$$-\frac{\mathrm{d[ABLM]}}{\mathrm{d}t} = k_{\mathrm{ABLM(obs,H)}} + k_{2\mathrm{H}}[\text{4-hydroxy-TEMPO−H}]$$

The role of the accessible H-atom in the reaction of ABLM with 4-hydroxy-TEMPO−H was further probed by deuterium isotope studies. ABLM was reacted with 4-hydroxy-TEMPO−D in deuterated HEPES buffer. The rate of reaction of ABLM with 4-hydroxy-TEMPO−D was decreased relative to that with 4-hydroxy-TEMPO−H and is shown to increase as a function of 4-hydroxy-TEMPO−D concentration in Figure 7B (diamonds). The best linear fit to the data has the vertical intercept $k_{ABLM(obs,D)}$ of 0.005 s^{-1}, which is the rate constant of decay of

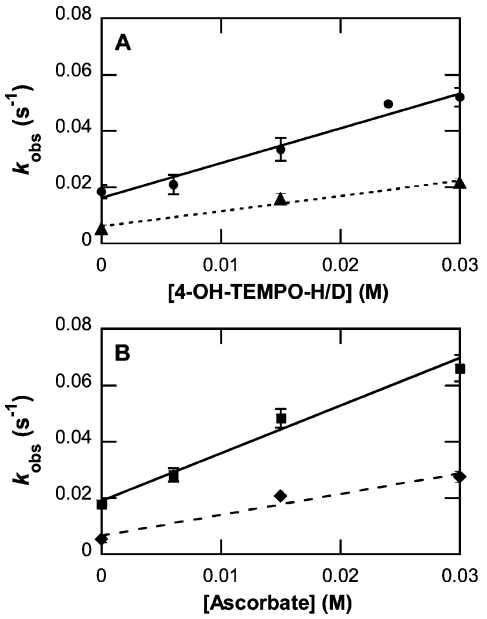

Figure 7. Plots of the observed rate constants of ABLM reaction as a function of substrate concentration at 20 °C. (A) Rate constants versus 4-hydroxy-TEMPO−H concentration (circles, solid line), and rate constants versus 4-hydroxy-TEMPO−D concentration (triangles, dashed line). (B) Rate constants versus $HAsc^-$ concentration (squares, solid line), and rate constants versus $DAsc^-$ concentration (diamonds, dashed lines).

ABLM in D_2O in the absence of substrate (vide supra), and yields a rate constant in D_2O, k_{2D}, of 0.40 ± 0.04 M^{-1} s^{-1} for the 4-hydroxy-TEMPO−H-dependent decay pathway. Thus, the reaction of ABLM with 4-hydroxy-TEMPO−H has a kinetic isotope effect (k_{2H}/k_{2D}) of 3.0 ± 0.4, again implicating H-atom involvement in the rate-determining step of the reaction.

At 4-hydroxy-TEMPO−H concentrations of 20 equiv and below, the CD spectrum of the final reaction mixture indicated that Fe^{III}BLM was the product. In the presence of 50 equiv or more of substrate, the product of ABLM decay was a salmon-pink-colored solution with a featureless CD spectrum between 11 300 and 33 300 cm^{-1} (900 and 300 nm), identifying it as Fe^{II}BLM. Thus, Fe^{III}BLM is formed during the early stages of the reaction but is subsequently reduced to Fe^{II}BLM by excess 4-hydroxy-TEMPO−H.[88]

3.1.3. Reaction with Ascorbate. Ascorbic acid is diprotic, with pK_1 = 4.1 and pK_2 = 11.8. At pH 7.8, the dominant form of ascorbate in solution is the monoanion. Ascorbate is widely used as a reducing agent and is known to be capable of both hydrogen-atom-transfer and proton/electron-transfer reactions. The homolytic bond dissociation energy (BDE) for the O−H bond at the carbon α to the carbonyl in ascorbate was calculated[89] to be similar to that of 4-hydroxy-TEMPO−H (∼72 kcal/mol). The weakness of this O−H bond suggests that ascorbate is also a good candidate as a H-atom donor.

ABLM was reacted with between 20 and 100 equiv of ascorbate. The rate of reaction increased linearly with increasing

(87) Caceres-Cortes, J.; Sugiyama, H.; Ikudome, K.; Saito, I.; Wang, A. H.-J. *Eur. J. Biochem.* **1997**, *244*, 818−828.
(88) 4-TEMPO−H has been shown react with Fe^{III}(Hbip) to give Fe^{II}(H_2bip) via an H-atom transfer that is formally PCET: Mader, E. A.; Larsen, A. S.; Mayer, J. M. *J. Am. Chem. Soc.* **2004**, *126*, 8066−8067.
(89) The O−H bond dissociation energy for ascorbate was calculated according to the reaction RH → R′ + H′ such that BDE(R −H) = [G_{solv}(R″) + G_{solv}(H″)]. The calculated BDE (using DFT with B3LYP) for ascorbate was 2 kcal/mol more exergonic than the calculated BDE for the weak O−H bond in 4-hydroxy-TEMPO−H.

Table 1. Thermodynamic Parameters for Possible Reaction Pathways[a]

	ΔE(gas)	ΔE(solv)	ΔG(solv)
reactivity of ABLM:			
homolytic O−O bond cleavage	25	22	13
direct H-atom abstraction	7	2	−10
heterolytic O−O bond cleavage[b]	104/51	25/26	15/16
reactivity of (BLM)Fe^{IV}=O:			
H-atom abstraction (second strand)	3	4	2

[a] All values in kcal/mol; for details see Computational Methods (section 2.2). [b] Values for two proton sources: for a solvated proton H^+(solv) with $\Delta G = -262.23$ kcal/mol and for an ammonia ion, NH_4^+.

amounts of ascorbate (Figure 7B (squares)). With the vertical intercept set at 0.018 s^{-1} ($k_{ABLM(obs,H)}$, vide supra), the slope of the best-fit straight line to the data yields a rate constant, k_{3H}, of 1.7 ± 0.1 M^{-1} s^{-1} for the ascorbate-dependent decay pathway. When varying concentrations of deuterated ascorbate were reacted with deuterated ABLM, a slower rate of reaction was observed. The rate constant for the ABLM reaction with deuterated ascorbate, k_{3D}, was found to be 0.61 ± 0.04 M^{-1} s^{-1} from the slope of the best linear fit (vertical intercept 0.006 s^{-1}, which is, within error, the value of $k_{ABLM(obs,D)}$, vide supra) to the kinetic data. The kinetic isotope effect is 2.8 ± 0.3, indicating that the reaction of ABLM with ascorbate also involves a hydrogen atom.

From CD data, at ascorbate concentrations of 20 equiv, the product of the ABLM reaction was Fe^{III}BLM. When higher concentrations of ascorbate were used, the product is Fe^{II}BLM, indicating that the excess ascorbate reduced the Fe^{III}BLM.

3.2. DFT Studies. Density functional calculations were carried out to gain further insight into the reaction pathways and mechanism of ABLM and its subsequent reactions.

3.2.1. Homolytic Cleavage and Direct H-Atom Abstraction by Activated Bleomycin. Two possible related reaction pathways are the homolytic cleavage of the O−O bond and the direct H-atom abstraction reaction from the DNA substrate by ABLM:

$$\text{Homolysis} \quad (\text{BLM})Fe^{III}-OOH \rightarrow (\text{BLM})Fe^{IV}{=}O + {}^{\bullet}OH$$

$$\text{Direct H-atom abstraction} \quad (\text{BLM})Fe^{III}-OOH + RH \rightarrow (\text{BLM})Fe^{IV}{=}O + H_2O + {}^{\bullet}R$$

Energetics. Table 1 presents calculated reaction energies for several reaction pathways of ABLM and (BLM)Fe^{IV}=O species. The homolytic cleavage of the O−O bond is energetically accessible, as shown in previous studies,[64,67] with a reaction free energy $\Delta G = 13$ kcal/mol.[90] This low energy is due in part to the relatively high stability of the Fe^{IV}=O species produced.

The direct H-atom abstraction reaction combines the homolytic O−O bond cleavage with an H-atom transfer from the substrate DNA to the leaving OH radical, forming H_2O and a C-4′ sugar radical. This reaction is exergonic, $\Delta G = -10$ kcal/mol. The lower reaction energy of this second reaction pathway compared to that of the homolytic cleavage derives from two contributions: the greater stability of the C-4′ radical compared to the hydroxyl radical •OH, and the formation of the stronger O−H bond of H_2O compared to the C−H bond of the substrate.

Thus, ABLM is thermodynamically competent to undergo direct H-atom abstraction. This reaction pathway is exergonic and energetically favored compared to the isolated homolytic cleavage of the O−O bond.

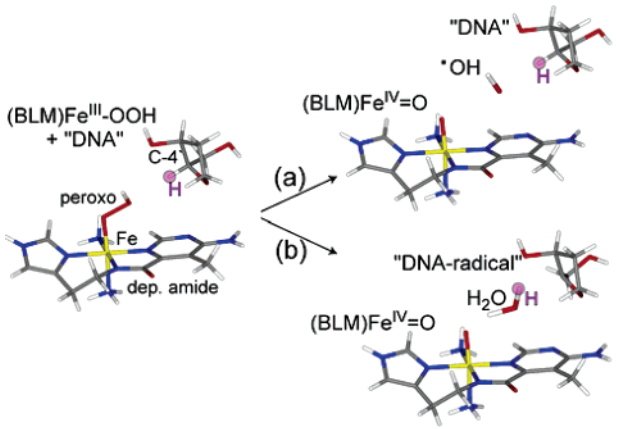

Figure 8. Structures of reactants and products of (a) homolytic O−O bond cleavage and (b) direct H-atom abstraction by ABLM.

Potential Energy Surface. In addition to the thermodynamics, the kinetics must be considered to evaluate the feasibility of this reaction pathway. Previous studies have shown that a homolytic O−O bond cleavage in low-spin Fe^{III}−OOH/R complexes does not have an additional kinetic barrier along the reaction coordinate.[66,67]

We have now investigated the potential energy surface for the direct H-atom abstraction reaction. The orientation of ABLM to DNA, modeled here by the deoxyribose sugar moiety, was adopted from solution NMR structures on (BLM)Co^{III}−OOH bound to oligonucleotides (for detailed information on the setup and computational procedures, see Computational Methods, section 2.2). Figure 8 shows reactants and products of the direct H-atom abstraction reaction by ABLM (Figure 8b) as well as the homolytic O−O bond cleavage (Figure 8a).

The reaction surface is two-dimensional: along one reaction coordinate the O−O bond is broken (r(O−O) axis in Figure 9); additionally, the 4′-H-atom is transferred from the substrate to the distal oxygen of the peroxo ligand along the second coordinate (r(O−H) axis in Figure 9).

In the left graph (Figure 9a), the reactants (ABLM + RH) with a small O−O distance, r(O−O) = 2.0 Å, and a large distance to the 4′-hydrogen, r(O−H) = 2.5 Å, are in front. On the right, with a large r(O−O) and a large r(O−H), are the products of a homolytic O−O bond cleavage. And in the back are the products of a direct H-atom abstraction, with a large r(O−O) and a short r(O−H) distance. The right graph (Figure 9b) shows the same plot rotated by ∼180°. Here the products of the direct H-atom abstraction are in front. The dark purple line (along one edge) traces the reaction coordinate of the homolytic O−O bond cleavage, as has been studied previously.[67] The substrate does not take part in this reaction; the distance from the peroxo to the 4′-hydrogen atom is large throughout the reaction, r(O−H) ≈ 2.5 Å.

The lowest energy path on this surface is traced with the red line: As the O−O bond is elongated, the energy rises steeply as the O−O σ-bond is gradually being broken. At r(O−O) ≈

(90) Slight differences in energy values between this and earlier publications [Lehnert, N.; Ho, R. Y. N.; Neese, F.; Que, L., Jr.; Solomon, E. I. *J. Am. Chem. Soc.* **2002**, *124*, 10810−10822. Solomon, E. I.; Decker, A.; Lehnert, N. *Proc. Natl. Acad. Sci. U.S.A.* **2003**, *100*, 3589−3594.] are due to different basis sets used. These differences are within error and do not change the overall picture.

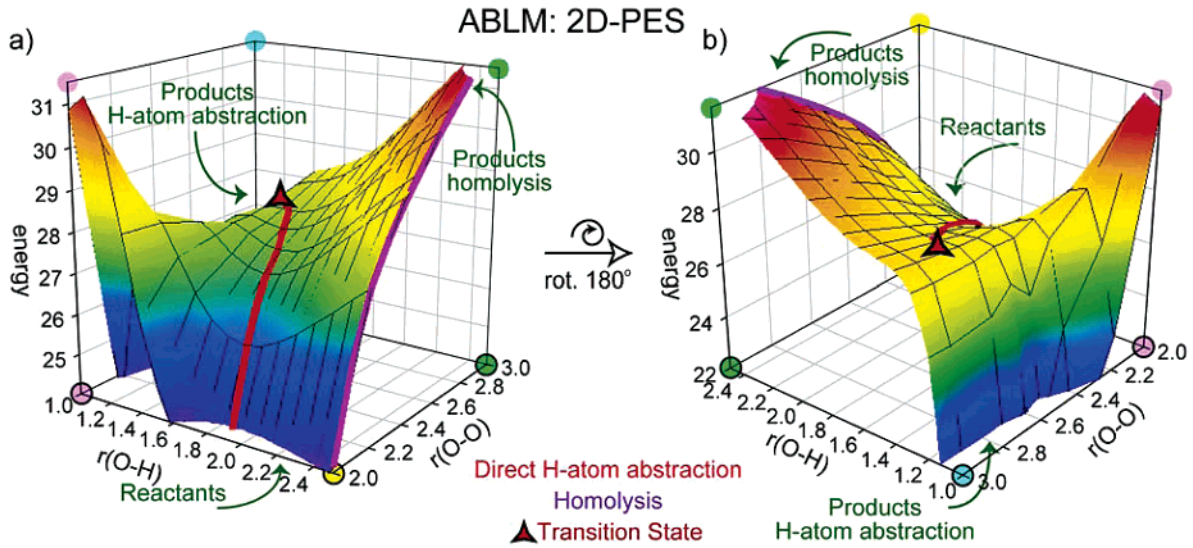

Figure 9. 2D potential energy surface for the direct H-atom abstraction by ABLM.

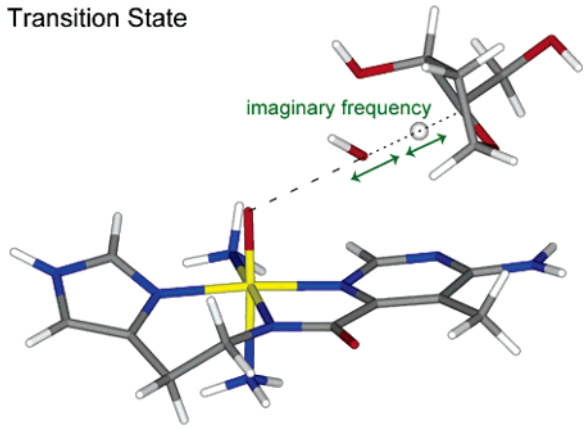

Figure 10. Transition-state structure for the direct H-atom abstraction of ABLM.

2.4 Å, the surface levels off. The distance between the distal oxygen and the 4′-hydrogen decreases, until at r(O−O) = 2.7 Å, the H-atom is spontaneously transferred and the products, H_2O and the sugar radical, form. The surface energy decreases steeply toward product formation (Figure 9b).

The transition state (TS) of this reaction is located at this saddle point (red triangle in plot). This calculated transition state (Figure 10) has only one negative frequency, $\nu = -195$ cm^{-1}. Its vibrational motion contains the oxygen and hydrogen atoms associated with the O−O cleavage and the H-atom transfer (C−H cleavage and O−H bond formation), as indicated in Figure 10. The relatively small value suggests a shallow saddle point, which is consistent with the potential energy surface. The activation energy for this H-atom abstraction reaction is E_a(gas) = 18 kcal/mol in the gas phase and E_a(solv) = 17 kcal/mol considering the solvent environment.[91]

The structure of the transition state gives further insight into the reaction mechanism. Table 2 shows structural and electronic parameters of reactants, TS, and products of this H-atom abstraction reaction by ABLM. The long O−O bond length, r(O−O) = 2.73 Å, indicates that the O−O bond is essentially broken at this point. The H−C bond is only modestly stretched, r(H−C) = 1.17 Å (from 1.10 Å in the reactants), and the O−H distance is still relatively long, r(O−H) = 1.45 Å. Thus, the transition state occurs late along the r(O−O) coordinate, but early with respect to the H-atom transfer, r(O−H).

Table 2. Changes of Structural and Electronic Parameters during H-Atom Abstraction by ABLM

	reactants	TS	products
structure			
r(O- -O)	1.50 Å	2.73 Å	
r(O- -H)		1.45 Å	0.98 Å
r(H- -C)	1.10 Å	1.17 Å	
spin densities			
Fe	0.90	1.12	1.12
O_{prox}	0.10	0.89	0.91
O_{dist}	0.00	−0.71	0.00
C-4′	0.00	−0.23	−0.82
H-atom	0.00	0.04	−0.01

Orbital Interactions and Electronic Structures. Analysis of the changes in the electronic structure along the reaction coordinate provides insight into the orbital contributions to the reaction mechanism.

This H-atom abstraction reaction is an electrophilic attack by ABLM on the electron density of the sugar C-4′−H bond. According to frontier molecular orbital (FMO) theory, a good electrophile requires low-lying unoccupied orbitals with large orbital coefficients on the attacking atom. For the hydroperoxo to become a good electrophile, the unoccupied O−O σ*-orbital (Figure 11, top) needs to decrease in energy and become concentrated on the distal oxygen, O_{dist}.[35] This occurs when the O−O bond is elongated: as the O−O σ-bond breaks, the energy of the O−O σ*-orbital decreases and the orbitals become polarized, i.e., localized on either the distal oxygen, O_{dist} (α-spin), or the proximal oxygen, O_{prox} (β-spin).

By the transition state this polarization is essentially complete: the low-lying unoccupied orbital character is localized on the distal oxygen in the α-spin manifold (Figure 11, center left). In the β-spin, the unoccupied orbital character concentrates on the proximal oxygen, one electron is partially transferred from the Fe^{III} to this oxygen (see increasing iron character in

(91) These values include zero-point and thermal corrections and have been determined from calculations with a large triple-ζ basis set (see the Computational Methods section for details).

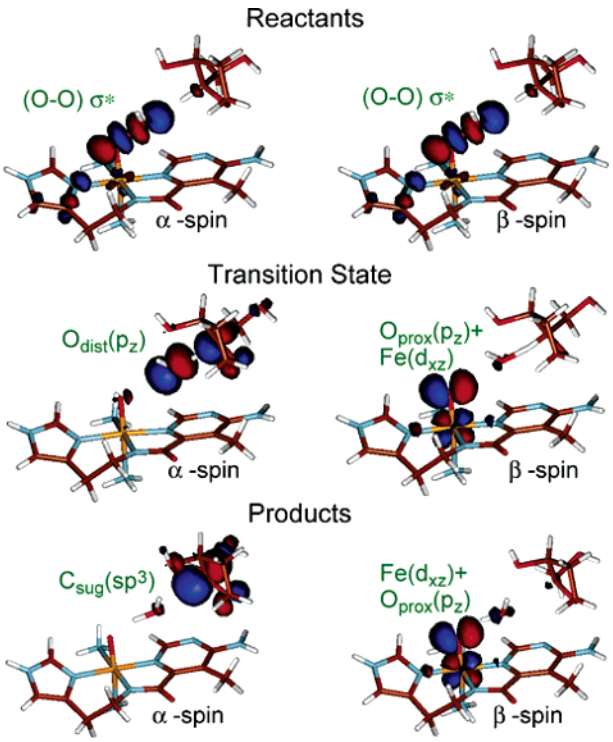

Figure 11. Correlation of molecular orbitals involved in electron transfer during the direct H-atom abstraction by ABLM (all orbitals shown are unoccupied).

the unoccupied orbital in Figure 11, center right), and the iron is formally oxidized to Fe^{IV}.

As the O−O bond is elongated, interactions between the proximal and distal oxygens decrease, while interactions between the distal oxygen and the C-4′ hydrogen increase. Thus, the distal oxygen is bound at all times and has strong interactions all along the reaction coordinate. No free hydroxyl radical, •OH, is generated.

The interaction of the distal oxygen with the substrate during the O−O bond cleavage has a stabilizing effect and lowers the energy relative to an isolated homolytic O−O bond cleavage. At the same O−O distance, the activation energy for an isolated homolytic cleavage is $\Delta E = 27$ kcal/mol, compared to $\Delta E_a = 17$ kcal/mol for the direct H-atom abstraction reaction.

After the transition state, the reaction proceeds energetically downhill, and the distal oxygen electrophilically attacks the C-4′ of the substrate to form the substrate radical and H_2O (Figure 11, bottom).

Thus, the direct H-atom abstraction reaction by ABLM has two components: the homolytic cleavage of the O−O bond occurs first, generating an Fe^{IV}═O species, followed by the H-atom transfer from the C-4′ to the distal oxygen. This reaction can be described as a concerted but nonsynchronous reaction mechanism.

3.2.2. H-Atom Abstraction by (BLM)Fe^{IV}═O: Initiation of Second-Strand Cleavage. Double-strand DNA cleavage is mediated by a single bleomycin molecule and occurs only in the presence of additional O_2, which provides the necessary oxidizing equivalents for the subsequent steps leading to the fragmentation of the DNA backbone.[55,92] The initial direct

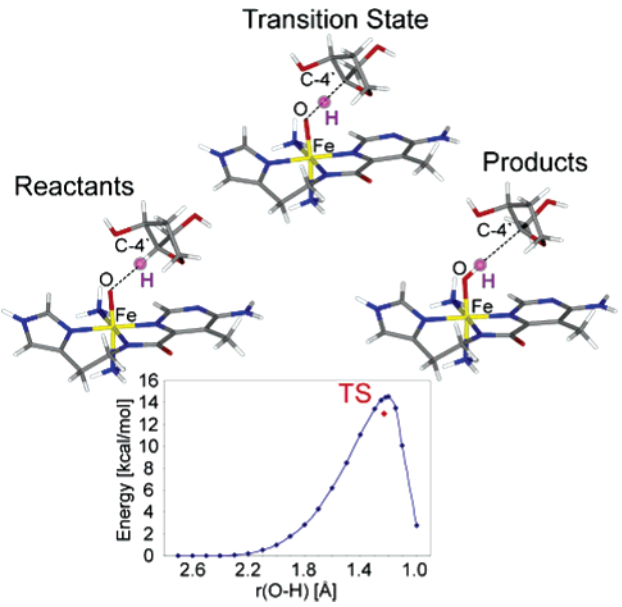

Figure 12. Structures and reaction scan of the hydrogen-atom abstraction reaction by (BLM)Fe^{IV}═O.

H-atom abstraction by ABLM would generate, in addition to the DNA-based radical, a high-valent (BLM)Fe^{IV}═O ($S = 1$) species. Similar Fe^{IV}═O species, having heme or non-heme ligand sets, are known to be very reactive and capable of C−H bond cleavage.[93−95] Here, we evaluate whether the bleomycin−Fe^{IV}═O species is capable of H-atom abstraction from the DNA sugar and thus could be the reactive species responsible for initiation of the second-strand cleavage event.

$$(\text{BLM})\text{Fe}^{\text{IV}}{=}\text{O} + \text{RH} \rightarrow (\text{BLM})\text{Fe}^{\text{III}}\text{OH} + {}^{\bullet}\text{R}$$

Energetics. Calculations of the thermodynamic parameters (Table 1) show that this reaction is thermoneutral, with a free reaction energy $\Delta G = 2$ kcal/mol. Here, neither solvent nor entropy has a strong effect on the reaction energies. Thus, abstraction of the 4′-hydrogen atom of a deoxyribose sugar moiety by the (BLM)Fe^{IV}═O species is thermodynamically accessible.

Reaction Coordinate. To further evaluate this reaction, we have followed the reaction pathway from the (BLM)Fe^{IV}═O ($S = 1$) reactants (Figure 12, left) through the 4′-hydrogen-atom transfer to form the (BLM)Fe^{III}−OH ($S = {}^1/_2$) and C-4′ sugar radical ($S = {}^1/_2$) products (Figure 12, right). Only one dimension, the position of the hydrogen atom, is needed for this profile. While the distance between the substrate and the Fe^{IV}═O was allowed to adjust, the 4′-hydrogen atom was moved stepwise toward the oxygen (decreasing r(O−H) along the reaction coordinate; Figure 12, bottom). With decreasing O−H distance, the energy gradually increases until the transition state is reached, after which the energy rapidly decreases toward the final products. It is a smooth transition, as can be seen from the changes, for example, in the spin densities or Fe−O distance (see Supporting Information).

(92) Absalon, M. J.; Wu, W.; Kozarich, J. W.; Stubbe, J. *Biochemistry* **1995**, *34*, 2076−2086.
(93) Kaizer, J.; Klinker, E. J.; Oh, N. Y.; Rohde, J.-U.; Song, W. J.; Stubna, A.; Kim, J.; Munck, E.; Nam, W.; Que, L., Jr. *J. Am. Chem. Soc.* **2004**, *126*, 472−473.
(94) Rohde, J. U.; Que, L. *Angew. Chem., Int. Ed.* **2005**, *44*, 2255−2258.
(95) Na, Y. O.; Suh, Y.; Mi, J. P.; Mi, S. S.; Kim, J.; Nam, W. *Angew. Chem., Int. Ed.* **2005**, *44*, 4235−4239.

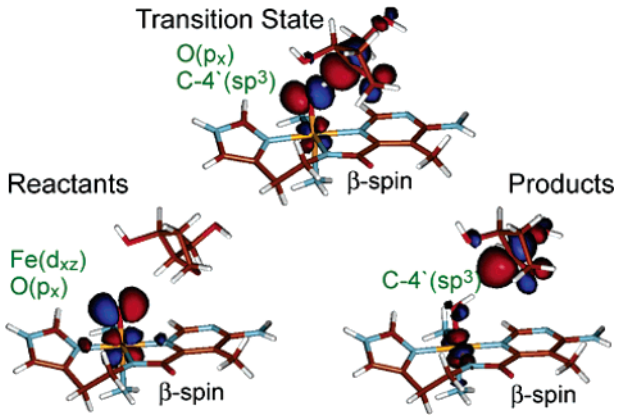

Figure 13. Correlation of the orbitals involved in electron transfer during the H-atom abstraction reaction by (BLM)Fe^{IV}=O (all unoccupied β-spin).

Table 3. Changes of Structural and Electronic Parameters during the H-Atom Abstraction Reaction by (BLM)Fe^{IV}=O

	reactants	TS	products
structure			
r(Fe—O)	1.65 Å	1.78 Å	1.84 Å
r(O- -H)		1.25 Å	0.98 Å
r(H- -C)	1.10 Å	1.30 Å	
spin densities			
Fe	1.23	0.96	0.96
O	0.82	0.58	0.06
C-4′	0.00	0.39	0.78
H-atom	0.00	−0.06	0.00

The structure of the transition state is shown in the center of Figure 12. It has only one imaginary frequency, $\nu = -1552$ cm^{-1}. The vibrational motion of this frequency corresponds to the hydrogen atom moving between the C-4′ and the oxygen atoms along the reaction coordinate. The relatively large value indicates a very steep potential energy surface around this saddle point, which is confirmed by the stepwise scan.

The activation energy for this reaction is E_a(gas) = 10 kcal/mol in the gas phase and E_a(solv) = 12 kcal/mol including solvent environment.[91] Thus, these calculations predict that the high-valent bleomycin−iron−oxo species is kinetically competent to cleave the 4′-C−H bond of a DNA sugar moiety with a relatively low activation barrier.

Orbital Interactions. Analysis of the changes in the electronic structure along the reaction coordinate provides further details about the reaction mechanism and insights into the origins of the relatively low activation barrier.

The reactant Fe^{IV}=O ($S = 1$), with an Fe-d$(xy)^2(xz/yz)^2$ occupation, is highly reactive and a good electrophile. According to FMO theory, large oxo coefficients in energetically low-lying unoccupied molecular orbitals result in good electrophilic attack. The strong and covalent iron−oxo π-bond results in large oxygen orbital coefficients in the low-lying half-occupied d(*xz*/*yz*) orbitals.[96] These orbitals are ideally set up for attack on the electron density on the C−H bond of the deoxyribose sugar substrate (Figure 13, left).

A comparison of structural and electronic parameters of the reactants, the transitions state, and the products (Table 3) shows that the TS is centered directly between reactants and products, with the hydrogen atom located between the oxygen and carbon atoms (r(O−H) = 1.25 Å and r(H−C) = 1.30 Å). This behavior is also reflected in the electronic structure: about half of the spin density of the final radical has been transferred to the C-4′ at the TS.

During this reaction, one electron is transferred along with the proton from the substrate C-4′ via the oxygen to the iron, which is reduced from Fe^{IV} to Fe^{III}, leaving a radical on the substrate. A correlation of the orbitals involved in this electron transfer is shown in Figure 13. Here we focus on the unoccupied orbitals and the transfer of the hole from the iron through the oxygen to the C-4′ on the substrate. The orbital correlation shows good orbital overlap along the reaction coordinate, allowing for rapid and smooth electron and hole transfer with a low activation barrier.

It is also noteworthy that, while the electron is transferred directly from the carbon of the substrate to the iron, the proton is transferred from the carbon to the oxygen. Thus, this "hydrogen-atom" transfer (HAT) is, in fact, better described as a proton-coupled electron transfer (PCET), where the proton and the electron are transferred simultaneously, but independently, to different acceptor atoms. This is reflected by the fact that the hydrogen atom does not carry spin density during its transfer. A similar mechanism has been observed for the H-atom abstraction reaction by a ferric−hydroxy species.[97]

Thus, the electrophilic properties of the iron−oxo reactant and the good orbital overlap along the reaction coordinate result in a low activation barrier and potentially fast H-atom abstraction reaction by (BLM)Fe^{IV}=O. This represents a reasonable mechanism for the initiation of second-strand DNA cleavage by the same BLM molecule.

3.2.3. Evaluation of Heterolytic O−O Bond Cleavage. It has been proposed that bleomycin utilizes the same oxygen intermediate as the heme enzyme cytochrome P450, a formally Fe^{V}=O intermediate called compound I (CpI), as the active oxidant in the H-atom abstraction reaction. Such a species might be formed via protonation and heterolytic cleavage of the O−O bond.

$$(BLM)Fe^{III}-OOH + H^+ \rightarrow \text{“}(BLM)Fe^{V}=O\text{”} + H_2O$$

Previous studies[35,64] have shown that, parallel to the heme CpI species, the putative "(BLM)Fe^{V}=O" is in fact better described as a (BLM$^{\bullet+}$)Fe^{IV}=O species, with an oxidized deprotonated amide moiety. To test whether the hole is clearly localized on the deprotonated amide or additional delocalization is possible, an extended model of the bleomycin ligand, which includes the whole metal-binding domain and part of the peptide linker (see details in Supporting Information), was used. The electronic structure of the "(BLM)Fe^{V}=O" species shows that the amide moieties in the linker region allow for some delocalization of the ligand hole. The spin density of ~0.8 that is located on the deprotonated amide bound to the iron center in the smaller model is spread equally over this deprotonated amide and an adjacent amide on the peptide linker. However, this extended delocalization is greatly reduced in even a low dielectric environment and does not lead to significant stabilization (*vide infra*).

To evaluate the heterolytic O−O bond cleavage as a possible alternative reaction pathway for ABLM, we have looked at the thermodynamics and a possible reaction pathway.

(96) Decker, A.; Rohde, J.-U.; Que, L., Jr.; Solomon, E. I. *J. Am. Chem. Soc.* **2004**, *126*, 5378−5379.

(97) Lehnert, N.; Solomon, E. I. *J. Biol. Inorg. Chem.* **2003**, *8*, 294−305.

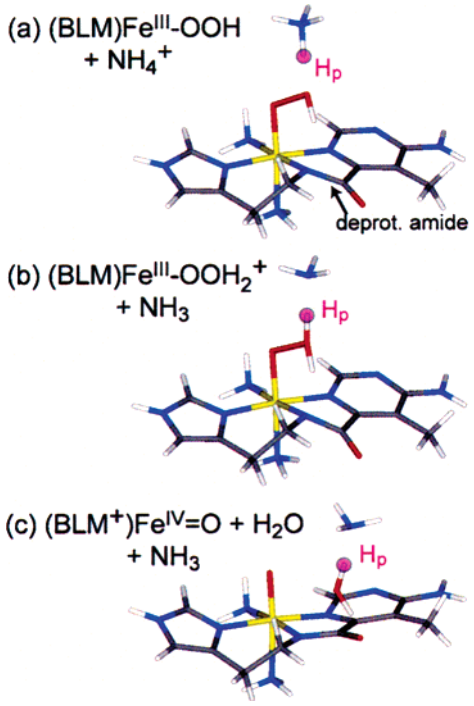

Figure 14. Protonation and heterolytic O−O bond cleavage of ABLM: (a) ABLM reactant, (b) protonated ABLM, and (c) products of heterolysis.

Energetics. The reaction energies have been calculated using either a solvated proton, H^+(solv),[83] or an ammonium ion, NH_4^+, which is a weak acid with pK_a = 9.25, as the proton source. The gas-phase energies in both cases are very high and unfavorable (Table 1). Because a highly charged species, [(BLM)Fe^V=O]$^{2+}$, is formed, the stabilization energy due to a solvent environment is significant and substantially lowers the reaction energies. The energies in a solvent are very similar for both proton sources, ΔE(solv) = 25 kcal/mol for H^+(solv) and ΔE(solv) = 26 kcal/mol for NH_4^+. The free reaction energies, $\Delta G(H^+)$ = 15 kcal/mol and $\Delta G(NH_4^+)$ = 16 kcal/mol, suggest that this reaction pathway is energetically accessible.[90] The free reaction energies are comparable to those of the isolated homolytic cleavage pathway but are ∼25 kcal/mol higher than the free energy for direct H-atom abstraction (ΔG = −10 kcal/mol).

The extended model of the bleomycin ligand changes the electronic structure of the "(BLM)Fe^V=O" species slightly, but the consequences for the energetics are not significant. Even though the energy for the heterolytic cleavage in the gas phase is ∼20 kcal/mol lower for the model with the linker region compared to the original model, inclusion of a solvent environment with a dielectric constant ϵ = 4.0 reduces the energy difference between the two models to 1 kcal/mol.

Potential Energy Surface. One possible pathway has been traced on the potential energy surface of the protonation and heterolytic O−O bond cleavage reaction (for a detailed reaction scan, see Supporting Information). Using NH_4^+ as the proton source, the reactants ABLM + NH_4^+ were optimized (Figure 14a). In a first scan, a proton was moved stepwise from the NH_4^+ to the distal oxygen of ABLM, which involved an energy increase of 15 kcal/mol. The O−O bond length was allowed to adjust at each step but did not change from the optimized value of r(O−O) = 1.5 Å. So, in contrast to calculations on cytochrome P450,[98,99] this protonated ABLM species (Figure 14b) does not cleave the O−O bond spontaneously. Its electronic structure is best described as a low-spin Fe^{III}−OOH_2^+.

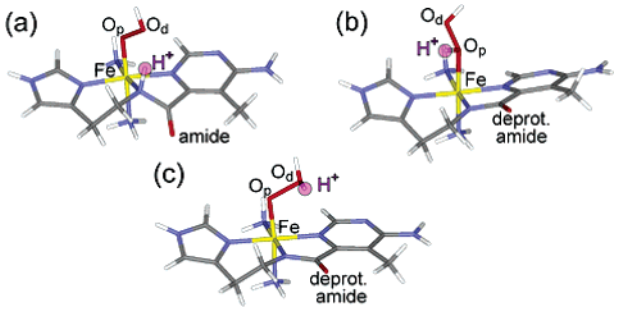

Figure 15. Three protonated ABLM structures: (a) protonation of deprotonated amide, (b) protonation of proximal oxygen, O_p, and (c) protonation of distal oxygen, O_d.

Table 4. Energies of ABLM Protonation Considering Two Proton Sources[a]

	ΔE(gas)	ΔE(solv)	ΔG(solv)
(a) protonation of amide	89/36	16/17	17/18
(b) protonation of O_{prox}	99/46	19/20	19/20
(c) protonation of O_{dist}	119/66	38/39	37/38

[a] All values in kcal/mol; for details see Computational Methods, section 2.2. Values for two proton sources: for a solvated proton H^+(solv) with ΔG = −262.23 kcal/mol and for an ammonia ion, NH_4^+.

In a second scan, the O−O bond of the Fe^{III}−OOH_2^+ was elongated stepwise, leading to the products (BLM$^{\bullet+}$)Fe^{IV}=O + H_2O + NH_3 (Figure 14c). This process is uphill by an additional 15 kcal/mol, resulting in an endothermic heterolysis process with a total energy increase of ∼30 kcal/mol.[100] No additional activation barrier was found along this reaction coordinate.

Protonated Activated Bleomycin. In the process of evaluating the protonation of ABLM as the possible first step in this heterolytic cleavage mechanism, three stable protonated species were found (Figure 15). All three species are energetically higher than ABLM + H^+(solv) or NH_4^+(solv) (Table 4); i.e., at neutral pH ∼ 7, all three would lose a proton to either the solvent or a nearby moderately weak basic residue.

Structure (a), a ferric−hydroperoxo complex with an amide instead of a deprotonated amide ligand (Figure 15), is the most stable of these three protonated species, energetically less favored compared to ABLM + H^+ by ∼17 kcal/mol. Protonation of the proximal oxygen of ABLM results in a hydrogen peroxide species, Fe^{III}−H_2O_2 (Figure 15b), with a long and weak Fe−O_{prox} bond, r(Fe−O_{prox} = 2.11 Å), which is energetically unfavorable by ∼19 kcal/mol. Alternatively, protonation of the distal oxygen of ABLM gives a stable Fe^{III}−OOH_2 complex (Figure 15c) which is almost 40 kcal/mol higher in energy than ABLM + H^+/NH_4^+. Thus, ABLM itself is a very weak acid and not protonated in a neutral environment.

4. Discussion

The experimental and computational results presented here indicate that ABLM is capable of direct H-atom abstraction and

(98) Harris, D. L.; Loew, G. H. *J. Am. Chem. Soc.* **1998**, *120*, 8941−8948.
(99) Ogliaro, F.; de Visser, S. P.; Cohen, S.; Sharma, P. K.; Shaik, S. *J. Am. Chem. Soc.* **2002**, *124*, 2806−2817.
(100) These energy values are derived from triple-ζ basis set calculations and include a solvent environment but no thermal, zero-point corrections. Inclusion of those parameters led to an energy value E(solv) = 26 kcal/mol, as shown in Table 1.

that this process is the energetically preferred pathway when compared to a homolytic or heterolytic O−O bond cleavage.

4.1. Experimental Results: Spectroscopy and Kinetics. Earlier studies on the reactions of BLM have determined that ABLM is the last iron intermediate detected prior to DNA strand cleavage. Past kinetic studies were limited by the weak absorption features of ABLM and relied on indirect methods, such as product analysis, to obtain kinetic data.[28,37,42] However, from Figure 3, ABLM has a characteristic CD feature at 22 200 cm^{-1} (450 nm) that is relatively strong even at low concentration (∼0.3 mM). By directly monitoring the change of intensity of this 22 200 cm^{-1} band, we were able to directly study the kinetics of the ABLM reaction. We find that the rate of ABLM decay is slower in D_2O than in H_2O and quantitatively yield a kinetic isotope effect (KIE, k_H/k_D) of ∼3.6 for ABLM decay. Thus, an H-atom must be involved in the rate-determining step of ABLM decay. From the 3D structure of (peplomycin)Co^{III}−OOH and Co^{II}BLM (Figure 6), there are at least two amide N−H bonds on the bithiazole peptide linker that are within 4 Å of the metal center and oriented toward the −OOH moiety. These N−H bonds are fast-exchanging and could provide the H/D atom that is involved in the ABLM decay reaction.

The rate of ABLM decay is accelerated when ABLM is reacted with 4-hydroxy-TEMPO−H or ascorbate, both of which act as hydrogen-atom donors and each of which has one relatively weak O−H bond (∼72 kcal/mol). The rate of ABLM reaction depends on substrate concentrations, and this dependence shows a deuterium isotope effect, $k_H/k_D \approx 3$, for both reactions. These results indicate that an H-atom is also involved in the rate-limiting step of the reaction of ABLM with substrates and establish that ABLM is capable of hydrogen-atom abstraction.

The magnitude and sign of the deuterium isotope effects (∼3) observed for ABLM reactions are indicative of a primary isotope effect; i.e., ABLM reactions involve an H−X bond cleavage. It has been proposed that the reaction of ABLM proceeds via protonation of the distal oxygen of the Fe^{III}−OOH moiety and heterolytic O−O bond cleavage to generate Fe^{V}=O and H_2O.[8,101] However, such heterolytic cleavage mechanisms, as observed in heme systems,[102] show a solvent deuterium isotope effect of $k_H/k_D \leq 2$,[103,104] which is not consistent with our experimental results. The observed deuterium isotope effect is also not associated with the proton/deuterium on the distal oxygen of the peroxo unit (−OOH vs −OOD), which should exhibit a secondary inverse isotope effect ($k_H/k_D < 1$) upon cleavage (homolytic or heterolytic) of the O−O bond and formation of H_2O.[105]

The deuterium isotope effects for the three reactions (ABLM decay, ABLM + 4-hydroxy-TEMPO−H, and ABLM + ascorbate) are similar, because the three reactions initially proceed via a similar mechanism. On the basis of ^{18}O isotope studies on ABLM decay, Burger and co-workers propose that O−O bond cleavage is part of the rate-limiting step of ABLM decay.[42] Stubbe et al. have observed isotope selection effects ($k_H/k_D \approx 2-7$) for the reaction of ABLM with DNA deuterium-labeled in the C-4′ position. [51,70] Those results, coupled with the primary deuterium isotope effect observed here, suggest that the rate-determining step of ABLM reactions involves an O−O bond cleavage coupled to a direct H-atom abstraction reaction.

4.2. Computational Results: Direct H-Atom Abstraction and Second-Strand Lesion. DFT calculations support the notion that ABLM, a low-spin ferric−hydroperoxo complex, is thermodynamically and kinetically competent to directly abstract the hydrogen atom from the C-4′ of the deoxyribose sugar moiety on the DNA strand. The calculated reaction free energy is $\Delta G = -10$ kcal/mol, and the activation energy $E_a(\text{solv}) = 17$ kcal/mol. Because of the nature of the transition state (vide infra), the dependence of the activation barrier on the C−H bond strength is expected to be small. This is supported by the good qualitative agreement of the calculated barrier with the experimentally obtained activation energy, $E_a(\text{exp}) = 9.3 \pm 0.9$ kcal/mol, for the decay of ABLM.

Mapping the two-dimensional potential energy surface for this reaction (Figure 9) has provided insight into its mechanism and yielded the geometric and electronic structures of the transition state. The transition state occurs late along the O−O reaction coordinate but early with respect to the H-atom transfer, r(O−H). The O−O bond is essentially broken (r(O−O) = 2.73 Å), while the C−H bond is only moderately stretched (r(C−H) = 1.17 Å). For the lowest energy pathway, the O−O bond needs to be significantly elongated, decreasing the energy of the O−O σ^*-orbital, to generate a good electrophile. The combined electrophilic attack and hydrogen-atom abstraction reaction is then exergonic.

The extent of the hydrogen-atom transfer in the transition state can be related to the magnitude of the kinetic isotope effect (KIE), k_H/k_D, by the Westheimer model.[106] The KIE approaches unity for transition states which resemble either the reactants or products. Intermediate transition-state structures are characterized by increasingly large isotope effects and reach a maximum for a symmetrical transition state. Using Pauling's relation for the length of partial bonds,[107] the geometric structure of the calculated transition state can be used to approximate the KIE. The transition state is early with respect to the C−H coordinate, with an only slightly elongated C−H bond, r(C−H) = 1.17 Å, and a long O−H distance, r(O−H) = 1.45 Å. The estimated KIE is $k_H/k_D = 3.1$ for this direct H-atom abstraction reaction by ABLM. This estimate agrees with the experimentally obtained KIE of $k_H/k_D \approx 3$ for ABLM decay, and for ABLM reactions with the substrates 4-hydroxy-TEMPO−H and ascorbate.

A comparison between the direct H-atom abstraction reaction and an isolated homolytic O−O bond cleavage (see section 3.2.1) shows that the interaction of the distal oxygen with the substrate during the O−O bond cleavage has a stabilizing effect and lowers the activation energy. Thus, a requirement for the

(101) Burger, R. M. *Metal−Oxo and Metal−Peroxo Species in Catalytic Oxidations*; Meunier, B., Ed.; Structure and Bonding 97; Springer: Berlin, 2000; pp 287−303.
(102) Sono, M.; Roach, M. P.; Coulter, E. D.; Dawson, J. H. *Chem. Rev.* **1996**, *96*, 2841−2887.
(103) Traylor, T. G.; Xu, F. *J. Am. Chem. Soc.* **1990**, *112*, 178−186.
(104) Aikens, J.; Sligar, S. G. *J. Am. Chem. Soc.* **1994**, *116*, 1143−1144.
(105) Since the product water has a stronger O−H/D bond and thus a larger vibrational force constant, (O−H/D), than the peroxide reactant, the transition state is likely to have a larger (O−H/D) force constant compared to the reactant. This translates into a greater activation barrier and hence a slower reaction rate for the lighter isotope, hydrogen, than for the deuterium and results in an inverse isotope effect: Klinman, J. P. *Adv. Enzymol.* **1978**, *46*, 415−494.
(106) Westheimer, F. H. *Chem. Rev.* **1961**, *61*, 265−273.
(107) Pauling, L. *The Nature of the Chemical Bond*; Cornell University Press: New York, 1960.

direct hydrogen-atom abstraction by the ferric−hydroperoxide, ABLM, seems to be the ready availability of the H-atom donor in order to drive the reaction toward the H-atom abstraction and not the homolytic O−O bond cleavage. In the BLM−DNA complex, it is known that only the C-4′−H bond is being broken, thus a well-oriented complex, as indicated by (BLM)Co^{III}−OOH−DNA NMR structures,[46,81] is needed for this reaction to proceed.

Hydrogen-atom abstraction by ABLM would generate a high-valent iron−oxo species, (BLM)Fe^{IV}═O, and a DNA-based C-4′ radical, which ultimately leads to DNA strand cleavage through two possible reaction pathways, depending on O_2 availability.[54−58] Along the O_2-independent pathway, which results only in single-strand DNA damage, the C-4′ radical is thought to be oxidized to a C-4′ carbocation.[108] Subsequent reaction with H_2O would yield a C-4′ ketone, leading to DNA strand scission under alkaline conditions. The high-valent Fe^{IV}═O species generated through the direct hydrogen-atom abstraction reaction by ABLM possesses high oxidizing power. Calculations show that a (BLM)Fe^{IV}═O species is able to oxidize the C-4′ radical to the proposed C-4′ carbocation while being reduced to the Fe^{III}−OH level with a free reaction energy, ΔG(solv) = −34 kcal/mol (for details, see Supporting Information). Thus, two sequential one-electron oxidations of the C-4′ of the deoxyribose sugar moiety can be carried out by ABLM, yielding a (BLM)-Fe^{III} species.

In the O_2-dependent pathway, the C-4′ radical is believed to react with dioxygen to form a peroxyl radical, ROO•, which after reduction to a peroxide can ultimately lead to formation of base propenal and DNA strand scission.[57,58,109] Reduction of the C-4′ peroxyl radical by the (BLM)Fe^{IV}═O to yield a (BLM•$^+$)Fe^{IV}═O species and R−OOH is calculated to be endergonic, with a free reaction energy, ΔG(solv) = +27 kcal/mol (see Supporting Information for details). The C-4′ peroxyl radical could alternatively abstract a hydrogen atom or perform addition reactions as occur in autoxidation radical chain reactions.

Double-strand DNA cleavage only occurs through the O_2-dependent pathway[92,110] and is believed to be responsible for BLM's cytotoxicity,[111] since it cannot be repaired by DNA polymerases, which require a template strand to function.[112] A single bleomycin molecule can mediate double-strand cleavage, and both are believed to be initiated by hydrogen-atom abstraction.[55,92] From the results in section 3.2.2, the (BLM)-Fe^{IV}═O ($S = 1$) intermediate generated by the first hydrogen-atom abstraction can function as the active oxidizing species, initiating the cleavage of the second DNA strand. One or both of the C-4′ radicals can react with O_2 to form a C-4′ peroxyl radical, which could react by either hydrogen-atom abstraction or oxidation of the other C-4′ radical via intra-DNA electron transfer, to yield a C-4′ carbocation and a C-4′ hydroperoxide. This mechanism does not require the reactivation of the iron intermediate.

As can be seen from the results in section 3.2.2, the second H-atom abstraction event, initiating the second DNA strand cleavage, can be carried out by the high-valent (BLM)Fe^{IV}═O intermediate. Several non-heme Fe^{IV}═O ($S = 1$) model complexes have been synthesized[94,113−116] and shown to be capable of similar H-atom abstraction reactions.[93,95] DFT calculations suggest their reactivity to be even higher than that of cytochrome P450.[117] The (BLM)Fe^{IV}═O species, similar to the previously characterized non-heme Fe^{IV}═O ($S = 1$) model complex,[96] has very strong σ- and π-donor Fe−O bonding interactions. Due to the covalent Fe−O π-donor bond a large amount of oxygen character is transferred to the low-lying unoccupied β-Fe(d_{xz}/d_{yz}) orbitals, making this oxo complex a very strong electrophile.

DFT calculations of the thermodynamics show that the hydrogen-atom abstraction reaction from the C-4′ of the deoxyribose sugar moiety of DNA by a (BLM)Fe^{IV}═O species is approximately thermoneutral (ΔG = 2 kcal/mol). Scanning of the reaction coordinate determined the transition state for this reaction and the activation energy, E_a(solv) = 12 kcal/mol (Figure 12). The transition state for this reaction is much more symmetrical than that for the first reaction of ABLM with DNA (r(C−H) = 1.3 Å and r(O−H) = 1.25 Å) and gives an estimated KIE k_H/k_D = 6. However, this second hydrogen-atom abstraction reaction is predicted to be significantly faster than the first reaction (i.e., ABLM with DNA), with a lower activation barrier (E_a(solv) = 12 kcal/mol vs E_a(solv) = 17 kcal/mol). Thus, no buildup of an intermediate is predicted or observed.

Importantly, the mechanistic model provides an attractive explanation of how a single molecule of BLM is able to cleave both strands of DNA while bound by intercalation of the bithiazole tail.[92] No reactivation after the initial C-4′ hydrogen-atom abstraction is required; all that is needed is an electron transfer between the DNA strands and a reorganization of the BLM metal binding region from the first to the second cleavage site.[6,118]

4.3 Comparison to Heme Systems. The iron−bleomycin system has often been compared to heme enzymes, i.e., to the heme monooxygenase cytochrome P450. The electronic structure of ferrous bleomycin does indeed show some heme characteristics,[10] and many reactions catalyzed by bleomycin are empirically similar to the reactivity of cytochrome P450. Thus, we briefly consider "heme-like" reaction pathways for bleomycin and draw a comparison.

In the generally accepted reaction mechanism of cytochrome P450, a low-spin ferric−hydroperoxo intermediate, often called compound 0 (Cp0), reacts with a proton, provided by the enzyme pocket, leading to the heterolytic cleavage of the O−O bond. This generates a (Por•$^+$)Fe^{IV}═O intermediate, compound I (CpI), which is believed to be a key active oxidizing species.[102] This

(108) Rabow, L. E.; Stubbe, J.; Kozarich, J. W. *J. Am. Chem. Soc.* **1990**, *112*, 3196−3203.
(109) McGall, G. H.; Rabow, L. E.; Ashley, G. W.; Wu, S. H.; Kozarich, J. W.; Stubbe, J. *J. Am. Chem. Soc.* **1992**, *114*, 4958−4967.
(110) Povirk, L. F.; Han, Y. H.; Steighner, R. J. *Biochemistry* **1989**, *28*, 5808−5814.
(111) Povirk, L. F. *Mutat. Res.* **1996**, *355*, 71−89.
(112) Klug, W. S.; Cummings, M. R. *Concepts of Genetics*, 5th ed.; Prentice Hall: Englewood Cliffs, NJ, 1997; pp 389−427.
(113) Rohde, J.-U.; In, J.-H.; Lim, M. H.; Brennessel, W. W.; Bukowski, M. R.; Stubna, A.; Munck, E.; Nam, W.; Que, L., Jr. *Science* **2003**, *299*, 1037−1039.
(114) Lim, M. H.; Rohde, J.-U.; Stubna, A.; Bukowski, M. R.; Costas, M.; Ho, R. Y.; Munck, E.; Nam, W.; Que, L., Jr. *Proc. Natl. Acad. Sci. U.S.A.* **2003**, *100*, 3665−3670.
(115) Klinker, E. J.; Kaizer, J.; Brennessel, W. W.; Woodrum, N. L.; Cramer, C. J.; Que, L. *Angew. Chem., Int. Ed.* **2005**, *44*, 3690−3694.
(116) Sastri, C. V.; Park, M. J.; Ohta, T.; Jackson, T. A.; Stubna, A.; Seo, M. S.; Lee, J.; Kim, J.; Kitagawa, T.; Munck, E.; Que, L.; Nam, W. *J. Am. Chem. Soc.* **2005**, *127*, 12494−12495.
(117) Kumar, D.; Hirao, H.; Que, L.; Shaik, S. *J. Am. Chem. Soc.* **2005**, *127*, 8026−8027.
(118) Keck, M. V.; Manderville, R. A.; Hecht, S. M. *J. Am. Chem. Soc.* **2001**, *123*, 8690−8700.

step of protonation and O−O bond cleavage is very fast, and a protonated Cp0, $Fe^{III}-OOH_2$, has not been experimentally observed. Calculations suggest that such a species is unstable and spontaneously reacts without a barrier to yield CpI and H_2O.[98,99] It is believed that the thiolate ligand trans to the peroxide causes a "push" effect,[119,120] worth ∼30 kcal/mol,[121] making Cp0 a strong base[98,99] and facilitating the heterolytic O−O bond cleavage.

ABLM is a low-spin ferric−hydroperoxo intermediate similar to Cp0. However, according to calculated thermodynamics, heterolytic O−O bond cleavage in BLM is less favorable compared to that in a model of cytochrome P450 by ∼70 kcal/mol.[64] In further contrast to the heme system, protonation of ABLM is energetically unfavorable, and a protonated (BLM)-$Fe^{III}-OOH_2$ species would not sponaneously cleave the O−O bond to generate a CpI equivalent and H_2O. Instead, this reaction is endergonic by ∼15 kcal/mol (section 3.2.3). Contributions to these energetic differences are the delocalization of the hole over the porphyrin ring, the axial thiolate ligand, and the extra negative charge in the cytochrome P450 system relative to the bleomycin complex.

A comparison of the heterolytic cleavage to other possible reaction pathways of ABLM shows that, even assuming no additional activation barrier, this heterolysis pathway is ∼10 kcal/mol higher than the highest point (transition state) of the direct H-atom abstraction pathway. Thus, bleomycin behaves very differently from heme systems, and we propose that it follows a different mechanistic pathway.

(119) Dawson, J. H.; Holm, R. H.; Trudell, J. R.; Barth, G.; Linder, R. E.; Bunnenberg, E.; C., D.; Tang, S. C. *J. Am. Chem. Soc.* **1976**, *98*, 3707−3709.
(120) Dawson, J. H.; Sono, M. *Chem. Rev.* **1987**, *87*, 1255−1276.
(121) Ogliaro, F.; de Visser, S. P.; Shaik, S. *J. Inorg. Biochem.* **2002**, *91*, 554−567.

4.4. Summary. The experimental and computational studies presented here on the reaction coordinate of activated bleomycin strongly support the low-spin (BLM)$Fe^{III}-OOH$ complex as the active oxidizing species and a direct hydrogen-atom abstraction as the reaction mechanism for the initial attack on DNA. The mechanism for double-strand cleavage by a single BLM molecule would then involve the $Fe^{IV}=O$ intermediate generated by the first reaction as the active species for the initial second H-atom abstraction reaction damaging the second DNA strand.

Thus, bleomycin does not follow the heme paradigm, which involves heterolytic O−O bond cleavage to generate a reactive CpI-like "$Fe^{V}=O$" intermediate. Instead, BLM uses low-spin $Fe^{III}-OOH$ and $Fe^{IV}=O$ species as the active oxygen intermediates. Interestingly, bleomycin also differs from the non-heme iron enzymes, which due to their weaker ligand fields have high-spin ground states for most ferrous, ferric, and ferryl species. Thus, bleomycin occupies its own space in the world of dioxygen-activating biological iron systems.

Acknowledgment. We thank Abhishek Dey and Prof. Dan Stack for helpful discussions. Financial support for this study was provided by the National Institutes of Health (GM-40392).

Supporting Information Available: Details on kinetic experiments; complete ref 72; complete 2D-PES of the direct H-atom abstraction by ABLM, including a contour plot; structure of extended ABLM model which includes part of the polypeptide linker region; energies and geometric and electronic structure details on all scans (H-atom by ABLM and by (BLM)$Fe^{IV}=O$, protonation, and heterolytic O−O bond cleavage); and Cartesian coordinates of the optimized structures. This material is available free of charge via the Internet at http://pubs.acs.org.

JA057378N